UNIVERSIDADE DE BRASÍLIA - UnB
INSTITUTO DE GEOCIÊNCIAS - IG
PROGRAMA DE PÓS-GRADUAÇÃO EM GEOLOGIA

MINERALOGIA E PETROLOGIA DA OCORRÊNCIA PALEOARQUEANA DE MAGNETITA VANADIFERA DE SÃO TOMÉ, NE DO BRASIL.

FELIPE VELÁSQUEZ RUIZ

DISSERTAÇÃO DE MESTRADO N° 384

Orientadora:

Prof[a]. Dra. Maria Emilia Schutesky Della Giustina

BRASÍLIA, 23 DE FEVEREIRO DE 2017

UNIVERSIDADE DE BRASÍLIA - UnB
INSTITUTO DE GEOCIÊNCIAS - IG
PROGRAMA DE PÓS-GRADUAÇÃO EM GEOLOGIA

MINERALOGIA E PETROLOGIA DA OCORRÊNCIA PALEOARQUEANA DE MAGNETITA VANADIFERA DE SÃO TOMÉ, NE DO BRASIL.

FELIPE VELÁSQUEZ RUIZ

Dissertação de mestrado submetida ao Programa de Pós-Graduação em Geologia, como parte dos requisitos necessários à obtenção do grau de Mestre em Geologia.

APROVADA POR:

_____

Maria Emilia Schutesky Della Giustina, Doutora, Professora Associada.

Instituto de Geociências - Universidade de Brasília – UnB

_____

Paola Ferreira Barbosa, Doutora, Professora Associada.

Instituto de Geociências - Universidade de Brasília – UnB

_____

Prof. Dr. Reinaldo Santana Correia de Brito, Doutor, Professor Adjunto.

Instituto de Geociências - Universidade Federal da Bahia – UFBA

BRASÍLIA, 23 DE FEVEREIRO DE 2017

“A mí deme un aguardiente,
un aguardiente de caña,
de las cañas de mis valles
y el anís de mis montañas.
No me den trago extranjero
que es caro y no sabe a bueno,
y porque yo quiero siempre
lo de mi tierra primero.
Ay! que orgulloso me siento
de haber nacido en mi pueblo”.

“Ay! que orgulloso me siento
de ser un buen COLOMBIANO¡¡”.

Autor: Rafael Godoy

Agradecimentos

Agradeço ao meu pai Agustín Velásquez Gallo e a minhas irmãs Yaneth, Susana e Renatha pelo apoio incondicional. Sem a sua colaboração não teria terminado o presente projeto de mestrado.

À minha orientadora Dra. Maria Emilia Schutesky Della Giustina por ter me dado a oportunidade de trabalhar com ela, agradeço a paciência, a tolerância e sobre tudo os novos conhecimentos geológicos e humanos adquiridos.

Ao meu co-orientador Dr. Claudinei Gouveia de Oliveira pelo conhecimento transmitido, especialmente no entendimento dos processos metalogenéticos.

Um especial agradecimento ao Dr. Elton L. Dantas pelas contribuições cientificas, especialmente no entendimento da geologia regional e local da área de estudo.

À Universidade de Brasília e em especial ao Instituto de Geociências por uma ótima acolhida aos estrangeiros. Agradeço também ao Laboratório de Geocronologia, ao Laboratório de Microssonda Eletrônica, ao Laboratório de Laminação e aos seus técnicos que de alguma forma contribuíram com as analises petrográficas, químicas e isotópicas do trabalho.

À Coordenação de Aperfeiçoamento de Pessoal de Nível Superior (Capes) pela concessão da bolsa de mestrado.

À empresa Eagle Star Mining Corp. por ter disponibilizado os furos de sondagem e financiado atividades de campo em São Tomé, Rio Grande do Norte.

Ao laboratório de geocronologia da USP, especialmente à Dra. Maria Helena pela colaboração no analises isotópico Ar-Ar em flogopita.

Aos meus amigos brasileiros de mestrado e doutorado da UnB, eles são o maior ganho da minha estadia dentro do Brasil.

Muito obrigado Alan Dantas Ferreira pela troca de ideias geológicas, acredito que você vai ser um dos maiores representantes da geologia do Brasil.

Ao meu amigo Carlos Arturo Moreno pelo suporte e companhia nesses dois anos em Brasília.

Finalmente, à minha amiga colombiana Angélica Maria Zapata, juntos começamos uma viagem desde Medellín-Colômbia até Brasília-Brasil, para cumprir o sonho de sermos mestres, que foi cumprido pela nossa dedicação e colaboração mútua. *Muchas gracias amiga, te quiero demasiado!!.*

Índice

Lista de Figuras

Lista de Tabelas

Resumo

As intrusões máficas acamadadas são formadas pela diferenciação de magmas basálticos, os quais foram gerados massivamente no Neoarquenho e Meso-Proterozóico a partir de plumas mantélicas emprazadas na crosta continental. Algumas intrusões máficas acamadadas hospedam corpos de minério de classe mundial de cromo, elementos do grupo da platina e óxidos de Fe-Ti-V, sendo algumas delas importantes províncias metalogenêticas. Até hoje, não se tem registro de intrusões máficas acamadadas do Paleoarqueano, no entanto, há registro de plumas em 3,5 Ga, como resultado dos primeiros episódios de crescimento de crosta Arqueana, fenômeno que poderia ter gerado o mais antigo registro de intrusões máficas acamadadas na terra. Os corpos mafico-ultramáficos acamadados de São Tomé são um grupo de rochas intrusivas desmembradas metamorfoseadas que tem uma estreita faixa de composição desde ol-websterito até hornblendito os quais hospedam minério de ilmenite-magnetita maciça, nas quais a magnetita tem conteúdo de V_2O_3 de 1,38 -1,98 wt.%. Os resultados analíticos de zircão usando LA-ICP-MS e os resultados de isótopos de Sm-Nd proporcionaram uma idade concordante de 3,5 Ga, para os corpos mafico-ultramáficos acamadados de São Tomé e um T_{DM} de 4,0 Ga. Também, a química mineral nas fases máficas apresentou altos teores de magnésio, em que a olivina apresentou teores até $Fo_{87,28}$ e 4605 ppm de Ni. Esses corpos acamadados sofreram um intenso processo de metamorfismo na fácies anfibolito e passaram então por três estágios de metassomatismo: (1) Um estágio metassomático rico em K-P-H_2O com abundante flogopita e clorita e também inclusões de apatita. (2) Um estádio metassomático rico em Ca-Na, no qual foram formados minerais do grupo do epidoto e sulfetos mais calcita, e (3) um estádio metassomático rico em K representado por bandas de flogopita, associado ao feldspato potássico, no qual a flogopita mostrou altas quantidades de titânio, com teores de TiO_2 de até 2,87 wt.%. Portanto, os dados químicos e isotópicos sugerem que os corpos mafico-ultramáficos acamadados de São Tomé foram gerados a partir de uma fusão parcial de uma fonte de peridotítica fértil em 4,0 Ga, que geram um magma ferropicrítico ou ferrobasáltico que cristalizou em 3,5 Ga, sendo o primeiro registro de crescimento crustal na plataforma sul-americana. Os óxidos de Fe-Ti-V foram gerados a partir de uma cristalização fraccionada e um processo de imiscibilidade, apesar de um elevado teor de voláteis na câmara magmática. Em seguida, os corpos em camadas sofreram um intenso metamorfismo no fácies anfibolito em 2,2 Ga e 0,6 Ga, ricas em H_2O representadas pela formação massiva de tschermakita o qual oxida o corpo do minério. Por fim, a intrusão acamadadas foi submetida a três estádios metassomáticos em altas temperaturas que remobilizaram Fe, Ti, Ni e Cr nos minérios enquanto o vanádio permaneceu imóvel.

Palavras chaves: Intrusões máficas acamadadas, minerais de Fe-Ti-V, 3.5 Ga, Província Borborema.

Abstract

Layered mafic intrusions are formed by differentiation of basaltic magmas, which were generated massively in Neoarchean and Meso-Proterozoic from mantle plumes emplaced in the continental crust. Some layered mafic intrusions host world-class ore bodies of chromium, platinum group elements and Fe-Ti-V oxides, being some of them important metallogenetic provinces. Hitherto, have not been reported layered mafic intrusions on Paleoarchean, nevertheless, there are plumes reported at 3,5 Ga, as a result of the first episodes of Archean crustal growth, phenomenon that could have generated the oldest record of layered mafic intrusion on earth. The layered mafic-ultramafic bodies of São Tomé is a group of metamorphosed dismembered intrusive rocks which has a narrow range of composition from ol-websterite to hornblendite and also host meter-sized massive ilmenite-magnetite lenses, in which magnetite has V_2O_3 contents of 1.38-1.98 wt.%. LA-ICP-MS zircon analytical results and Sm-Nd isotopes gave a concordant age of 3.5 Ga, for the layered mafic-ultramafic bodies of São Tomé and a T_{DM} age of 4.0 Ga. Also, mineral chemistry in the mafic phases displayed high tenors of magnesium, in which olivine showed contents up to $Fo_{87.28}$ and 4605 ppm of Ni. These layered bodies were metamorphosed in the brasiliano cycle and then passed by three stages of metasomatism: (1) A K-P-H_2O-rich metasomatic stage with abundant phlogopite and chlorite and also inclusions of apatite. (2) A Ca-Na-rich metasomatic stage, in which were formed epidote group minerals and sulfides plus calcite, and (3) A K-rich metasomatic stage represented by phlogopite bands, associated with potassium feldspar, in which phlogopite showed huge amounts of titanium, with TiO_2 contents up to 2.87 wt.%. Therefore, chemical and isotopic data suggests that the layered mafic-ultramafic bodies of São Tomé were generated from a partial fusion of a fertile peridotite source at 4.0 Ga, which generate a ferropicritic or ferrobasaltic magma that crystalized at 3.5 Ga, been the first register of continental growth in the south American platform. Fe-Ti-V oxides ores were generated from a fractional crystallization and an immiscibility process, despite a high content of volatiles in the magmatic chamber. Then, the layered bodies underwent an intense metamorphism in amphibole facies at 2.2 Ga and 0.6 Ga, rich in H_2O represented by the massive formation of Tschermakite that oxide the ore body. By last, the layered intrusion was submitted to three metasomatic stages at high temperatures that remobilized Fe, Ti, Ni and Cr in the ores while vanadium remained immobile.

Keywords: Layered mafic intrusion, Fe-Ti-V ores, 3.5 Ga, Borborema Province.

CAPÍTULO 1

I. Introdução

A Faixa Seridó está localizada na porção setentrional da Província Borborema (Almeida *et al.* 1981), sendo constituída por sequências metassedimentares Neoproterozoicas depositadas sobre um embasamento gnáissico Paleoproterozoico (De Souza *et al.* 2007) posteriormente intrudida por um grupo de granitoides Edicarianos e Cambrianos entre 635-541 Ma (Do Nascimento *et al.* 2015). Aflorante na parte norte da Faixa Seridó, encontra-se um grupo de corpos máficos a ultramáficos descritos pelo Serviço Geológico do Brasil na Folha Lajes SB.24-X-D-VI (Costa e Dantas, 2014), portadores de óxidos de ferro e titânio, hospedados em ilmenita e magnetita, os quais são importantes indicadores petrogenéticos, além de possuírem grande importância industrial.

Especificamente, na localidade de Novo Mundo, município de São Tomé, afloram cinco corpos máfico-ultramáficos acamadados, deformados e metamorfisados no fácies anfibolito, os quais foram descritos inicialmente por Costa *et al.* (2014). No referido trabalho, é descrita uma ocorrência de minério de ilmenita e titanomagnetita em níveis maciços, contendo elevados teores de vanádio e que segue o *trend* NNE da Falha de Santa Mônica. Para o detalhamento desse prospecto mineral, foram realizados cinco furos de sondagem pela *Eagle Star Mining Corporation* na área dessas ocorrências. Os teores do depósito ainda estão sendo avaliados.

Na descrição dos furos de sonda foi possível observar o intenso processo de metassomatismo, caracterizado pela presença pervasiva de flogopita mais clorita, truncando tanto o acamamento do minério quanto o bandeamento de anfibólio. A ação dos processos metamórficos e metassomáticos em estágios diferentes pode ter obliterado as assinaturas químicas magmáticas originais.

A dissertação segue a orientação do Programa da Pós-graduação em Geologia da Universidade de Brasília. Os resultados e discussões são apresentados em formato de artigo científico intitulado *"The 3,5 Ga layered mafic-ultramafic bodies of São Tomé"* e que será submetido preferencialmente à revista especializada *Precambrian Research.*

II. Objetivos

A dissertação aborda (1) a petrogênese dos corpos máfico-ultramáficos acamadados de São Tomé, (2) a gênese dos óxidos de Fe-Ti-V, (3) o metamorfismo sobreposto ao processo ígneo e (4) o papel do metassomatismo como processo responsável pela mobilização dos elementos maiores, menores e traços no minério.

III. Localização e acesso

A área de estudo situa-se na porção central do município de São Tomé, a 10 km ao sul da Mina de Au-W de Bonfim, no Estado de Rio Grande do Norte (Fig. 1a), compreendendo uma área de 19 Km^2 (Fig. 1b).

O acesso a partir da cidade de Natal é feito através da rodovia BR-304, sentido oeste até chegar à RN-203, que permite o acesso direto ao Município de São Tomé, com um percurso total de 100 km. O acesso à ocorrência de Fe-Ti-V é feito por meio da RN-203, no sentido oeste, por 3 km até a estrada de terra que dá acesso (10 km) a localidade de Novo Mundo (Fig. 1b).

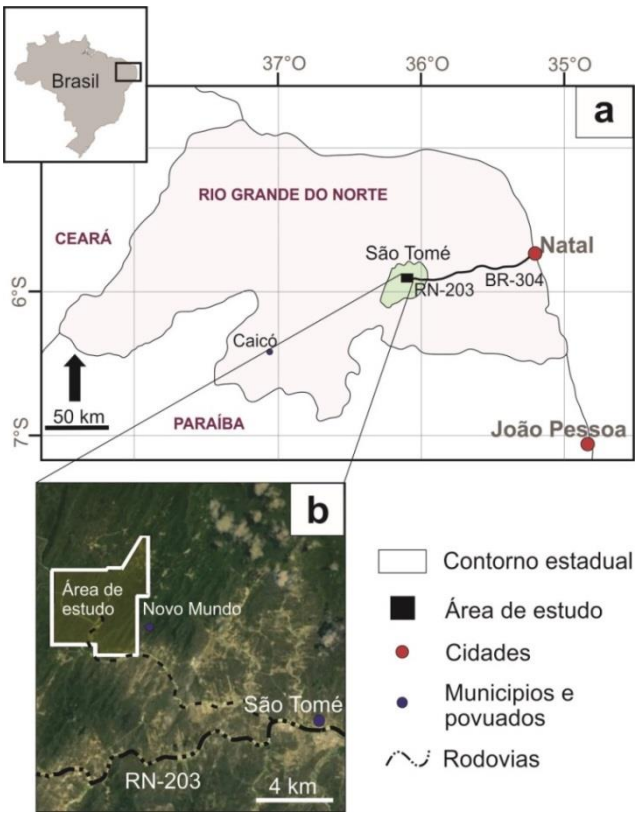

Fig. 1. Localização e vias de acesso da área de estudo. (a) Sentido Natal-São Tomé. (b) Sentido São Tomé-Novo Mundo.

IV. Justificativa

As intrusões máficas acamadadas estão compostas por rochas cumuláticas formadas por diferenciação de magmas basálticos dentro da crosta continental, que posteriormente vão ser expostas à superfície por erosão (Winter, 2001). Por outra parte intrusões máficas acamadadas que hospedam óxidos de cromo, ferro ou titânio são formados especificamente a partir de magmas ferropicríticos ou ferrobasálticos ricos em titânio (Liu et al. 2015; Pang et al. 2008), gerados por fusão parcial de um manto peridotítico. Assim, dependendo da configuração geológica e química, as intrusões máficas acamadadas podem ser hospedeiras de depósitos de classe mundial de cromita, magnetita, ilmenita ou elementos do grupo dos platinoides, sendo alguns desses depósitos importantes províncias metalogenéticas como o Complexo Bushbeld na África do Sul ou ou A Província ígnea Emeishan na China.

Os trabalhos de exploração mineral na área de Novo Mundo, desenvolvidos pela empresa *Eagle Star Mining Corporation* e pelo programa de mapeamento da folha Lajes do Serviço Geológico do Brasil, possibilitaram a descoberta de ocorrências de minério maciço de magnetita e ilmenita em corpos máfico-ultramáficos acamadados, com elevados teores de vanádio. Os dados de campo associados aos teores indicam um relevante potencial para depósitos de Fe-Ti-V, com uma paragênese mineral semelhante aos depósitos de classe mundial conhecidos. Na descrição dos furos de sonda foi observada uma foliação marcada por anfibólios e um processo de metassomatismo, com formação de flogopita e clorita, truncando tanto o acamamento do minério quanto o bandeamento de anfibólio.

Assim, este trabalho pretende abordar a origem dos corpos máfico-ultramáficos de São Tomé, elucidar a gênese dos óxidos de Fe-Ti-V, o metamorfismo sobreposto ao processo ígneo e o papel do metassomatismo, especialmente nas assinaturas químicas.

Magnetita

Magnetita (Fe_3O_4) é um importante indicador petrogenético com aplicações em geofísica, petrologia ígnea, estudos de proveniência e exploração mineral (Nadoll *et al.* 2014). A magnetita pertence ao grupo do espinélio, com uma estequiometria geral da forma "AB_2O_4" (Fleet, 1981), em que "A" representa os cátions bivalentes em ligação octaédrica como Mg, Fe^{2+}, Ni, Mn, Co ou Zn (Fig. 2), e "B" representa o cátion trivalente em ligação octaédrica como Al, Fe^{3+}, Cr, V, Mn ou Ga. O Ti, com carga 4+, pode ocupar o lugar de "B" quando a

substituição é acoplada com um cátion bivalente (Fig. 2a). Uma forma de analisar a composição mineral e as soluções sólidas é por meio dos óxidos maiores, devido ao fato de que a magnetita, acima de 600°C, tem uma solução sólida com o ulvospinélio (Fig. 2b). Assim, é importante determinar com exatidão o teor de TiO_2, FeO e Fe_2O_3, como também os elementos traços, o que permite analisar aspectos metalogenéticos relacionados a processos de cristalização fracionada ou assimilação (Liu *et al.* 2015; Zhou *et al.* 2005; Pang *et al.* 2008).

As possíveis fases minerais estão dadas pelas reações das Equações 1 e 2 (Ghiorso e Sack, 1991). Segundo a Equação 1, magnetita e ilmenita são minerais que crescem em paragênese, dupla mineral que forma depósitos minerais de classe mundial em corpos máficos acamadados tipo Bushveld na África do Sul, ou nos depósitos de Fe-Ti-V encontrados na Província Ígnea Emeishan, SW China (Eales and Cawthorn, 1996; Liu *et al.* 2015).

$$\mathbf{Fe2O3} + \mathbf{Fe2TiO4} = \mathbf{Fe3O4} + \mathbf{FeTiO3} \qquad (\mathbf{Eq.1})$$

$$\text{Hematita} + \text{Ulvospinel} = \text{Magnetita} + \text{Ilmenita.}$$

$$\mathbf{2Fe2O3} + \mathbf{6FeTiO3} = \mathbf{6Fe2TiO4} + \mathbf{O2} \qquad (\mathbf{Eq.2})$$

$$\text{Hematita} + \text{ilmenita} = \text{Ulvospinel} + \text{Oxigenio}$$

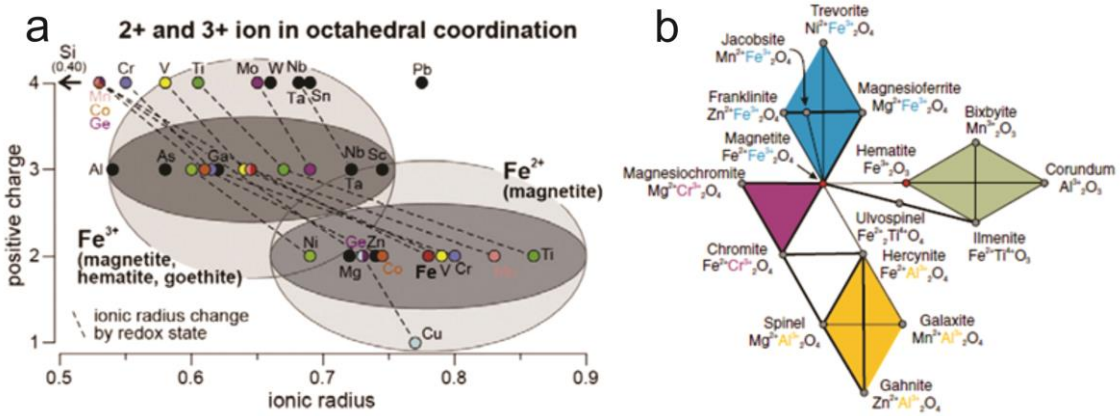

Fig. 2. Química básica do grupo do espinélio: (a) Raio iónico em Angstrom vs. Carga catiônica para sítios octaédricos (Nadoll *et al.* 2014). (b) Representação esquemática dos membros extremos do grupo do espinélio em azul mais a solução sólida completa com o ulvospinélio, representado pela linha espessa entre magnetita e ilmenita. Soluções sólidas incompletas estão sendo representadas pelas linhas finas (Dupuis e Beaudoin, 2011).

V. Métodos

O presente projeto de dissertação de mestrado foi desenvolvido em seis etapas: (1) revisão bibliográfica da província Borborema com foco na faixa Seridó e processos de formação de corpos máfico-ultramáficos acamadados no mundo e seus depósitos, (2) trabalho de campo no Município de São Tomé, Rio Grande do Norte, Brasil, (3) análises petrográficas, (4) química mineral, (5) geocronologia a partir dos métodos U-Pb em zircão, Sm-Nd em rocha total e Ar-Ar em grãos de flogopita. E, por fim, (6) interpretação de resultados e elaboração do documento final de dissertação.

O trabalho de campo foi desenvolvido em julho de 2015 e envolveu a descrição de cerca de 400 m de furos de sondagem disponibilizados pela empresa *Eagle Star Mining Corporation*, além de trabalho de campo. A pesquisa teve como base cartográfica o mapa da folha Lajes SB.24-X-D-VI da CPRM. A partir dos furos de sondagem, foram coletadas trinta e duas amostras e confeccionadas lâminas delgadas-polidas por amostra. As lâminas que conservaram melhor os processos magmáticos, metamórficos e metassomáticos foram analisadas em Microssonda Eletrônica modelo JEOL JXA-8230 do Instituto de Geociências da Universidade de Brasília. Os minerais selecionados pelas análises de química mineral comprendem olivina, o grupo do piroxênio, o grupo do anfibólio, magnetita, ilmenita, flogopita e clorita. Os diagramas de química mineral foram feitos em *Microsoft Excel* 2010 e editados em *CorelDRAW* X7. Para complementar o analises de química mineral, foi usado o programa QUILF, usando a dupla mineral magnetita-ilmenita pela obtenção da fugacidade do oxigênio e a temperatura do minério.

As análises isotópicas U-Pb em zircão e Sm-Nd em rocha total foram obtidos pelo Laboratório de Geocronologia da Universidade de Brasília.

CAPITULO 2

Paper to be submitted to Precambrian Research

THE 3,5 GA LAYERED MAFIC-ULTRAMAFIC BODIES OF SÃO TOMÉ, NE BRAZIL: MINERALIZATION, METAMORPHISM AND METASOMATISM.

Abstract

Layered mafic intrusions are formed by differentiation of basaltic magmas, which were generated massively in Neoarchean and Meso-Proterozoic from mantle plumes emplaced in the continental crust. Some layered mafic intrusions host world-class ore bodies of chromium, platinum group elements and Fe-Ti-V oxides, being some of them important metallogenetic provinces. Hitherto, have not been reported layered mafic intrusions on Paleoarchean, nevertheless, there are plumes reported at 3,5 Ga, as a result of the first episodes of Archean crustal growth, phenomenon that could have generated the oldest record of layered mafic intrusion on earth. The layered mafic-ultramafic bodies of São Tomé is a group of metamorphosed dismembered intrusive rocks which has a narrow range of composition from ol-websterite to hornblendite and also host meter-sized massive ilmenite-magnetite lenses, in which magnetite has V_2O_3 contents of 1.38-1.98 wt.%. LA-ICP-MS zircon analytical results and Sm-Nd isotopes gave a concordant age of 3.5 Ga, for the layered mafic-ultramafic bodies of São Tomé and a T_{DM} age of 4.0 Ga. Also, mineral chemistry in the mafic phases displayed high tenors of magnesium, in which olivine showed contents up to $Fo_{87.28}$ and 4605 ppm of Ni. These layered bodies were metamorphosed in the brasiliano cycle and then passed by three stages of metasomatism: (1) A K-P-H_2O-rich metasomatic stage with abundant phlogopite and chlorite and also inclusions of apatite. (2) A Ca-Na-rich metasomatic stage, in which were formed epidote group minerals and sulfides plus calcite, and (3) A K-rich metasomatic stage represented by phlogopite bands, associated with potassium feldspar, in which phlogopite showed huge amounts of titanium, with TiO_2 contents up to 2.87 wt.%. Therefore, chemical and isotopic data suggests that the layered mafic-ultramafic bodies of São Tomé were generated from a partial fusion of a fertile peridotite source at 4.0 Ga, which generate a ferropicritic or ferrobasaltic magma that crystalized at 3.5 Ga, been the first register of continental growth in the south American platform. Fe-Ti-V oxides ores were generated from a fractional crystallization and an immiscibility process, despite a high content of volatiles in the magmatic chamber. Then, the layered bodies underwent an intense metamorphism in amphibole facies at 2.2 Ga and 0.6 Ga, rich in H_2O represented by the massive formation of Tschermakite that oxide the ore body. By last, the layered intrusion was submitted to three metasomatic stages at high temperatures that remobilized Fe, Ti, Ni and Cr in the ores while vanadium remained immobile.

Keywords: Layered mafic intrusion, Fe-Ti-V ores, 3.5 Ga, Borborema Province.

1. Introduction

Layered mafic intrusions consist of cumulates rocks formed by differentiation of basaltic magmas within the continental crust, what will later be exposed at the surface by erosion (Winter, 2001). Some layered mafic intrusions host world-class ore bodies of chromite, platinum group elements, magnetite and ilmenite (Cawthorn, 1996), being some of them important metallogenetic provinces like Bushveld Complex or Emeishan Large Igneous Province (Eales and Cawthorn, 1996; Liu et al., 2015; Zhou et al., 2005), therefore different works have been developed to better elucidate the petrogenesis and metallogenesis of these intensely differentiated bodies. Different mechanisms have been proposed for the formation of these polymetalic deposit, and specifically three mechanism have been suggested for the formation of Fe-Ti-V layers (Charlier et al., 2015; Liu et al., 2015; Vantongeren and Mathez, 2012; Zhou et al., 2005): (1) the Fe-Ti enrichment may be the final feature of an intense differentiation process from basaltic liquids. (2) By an assimilation process between a basaltic liquid and continental rocks with high iron and titanium content, such as Banded Iron Formation. (3) From immiscible liquids rich in Fe-Ti-V±(P).

Layered Mafic intrusion were generated massively in Neoarchean and Meso-Proterozoic (Cawthorn, 1996; Charlier et al., 2015). However, different mafic intrusions had formed throughout time from mantle plumes emplaced in the continental crust as the case of Panzhihua intrusion, SW China at 260 Ma (Zhou et al., 2005) or the Skaergaard intrusion, east Greenland at 55 Ma (McBirney, 1996). Hitherto, have not been reported layered mafic intrusions on Paleoarchean, nevertheless, there are plumes reported at 3,5 Ga (Pearson et al., 1995; Peltonen et al., 2006), and also mantle plumes is one of the models for the origin of the archean subcontinental lithospheric mantle (Rollinson, 2010), been 3.5 Ga a key age for the Archean crustal growth (Peltonen et al., 2006), phenomenon that could have generated the oldest record of layered mafic intrusion on earth.

There is a group of layered mafic-ultramafic bodies at the municipality of São Tomé, Rio Grande do Norte state, NE Brazil, which host meter-sized massive magnetite-ilmenite lenses. The bodies crops out over an area of 658000 m^2 at the septentrional portion of the Seridó Belt, Borborema Province (Fig. 3). The main intrusion of this suit was drilled from an extensive drilling program conducted by Eagle Star Mining Corp. At the time of logging, was identified an intense metasomatism with a pervasive formation of chlorite and phlogopite, process that could be changed the original chemical signature of this deposit. With the above, this paper will deal with the petrogenesis of the layered mafic-ultramafic bodies of São Tomé, the mechanism that formed its Fe-Ti-V layers, the metamorphism superimposed on the igneous layers, as well as the role of the metasomatism as a responsible process for a possible element migration.

2. Geological Background

2.1. Regional Geology

The Borborema Province, located on northeast Brazil (Almeida et al., 1981), is the result of the tectonic convergence between the São Luis-West Africa and São Francisco-Congo cratons in the Brasiliano/Pan-African orogeny (de Sa et al., 1995), as part of the West Gondwana assembly. The province consists of metasedimentary sequences which were deposited over Archean to Paleoproterozoic gneissic basement (Dantas et al., 2014) and were subsequently intruded by a cluster of Ediacaran to Cambrian (635-541Ma) granitoids (Do Nascimento et al., 2015). The tectonic configuration of the Borborema Province consist on a complex system of large crustal-scale shear zones that form a set of independent domains (Arthaud et al., 2008; Costa & Dantas, 2014), therefore, the province is divided into five major tectonic domains (Van Schmus et al., 2003), three of them in the eastern part (Fig. 3) as follows: the southern domain, between the Pernambuco shear zone and the São Francisco Craton; the central or Zona Transversal Domain, between the Patos and Pernambuco shear zones; and the Rio Grande do Norte domain, to the north of the Patos shear zone. The remaining domains are located at the far west side and are Central Ceará and Médio Coreau.

The studied area is located on the Rio Grande do Norte Domain, which comprises: (1) Archean orthogneisses of the Granjeiro and São José do Campestre massifs. Both of them represent the first record of continental growth in the province. São José do Campestre massif consist in a set of igneous complexes from metagabbro to metagranodiorite, in which Bom Jesus tonalite gneiss is rather prominent because contains one of the oldest records of continental crust present in South America (Dantas et al., 2004; Dantas et al., 2014), with U-Pb ages up to 3.4 Ga. (2) Paleoproterozoic meta-plutonic rocks of the Caicó Complex. This complex is composed of a meta-volcano-sedimentary unit that mainly consist of garnet-bearing paragneisses and a metaplutonic unit represented by quartz diorite, metagabbro and metaultramafic rocks that were emplaced around 2.2 Ga (De Souza et al., 2007). (3) Meta-supracrustal sequences of the Paleoproterozoic Orós-Jaguaribe belt and the Neoproterozoic Seridó group, which includes the Seridó, Equador and Jucurutú Formations, deposited over the previous basement. The Seridó Group was deposited over the Seridó Belt (Fig. 3) that limits with the São José do campestre massif by the Picuí-João Câmara Shear Zone. (4) A group of Ediarcan to Cambrian granitic batholiths, stocks and dykes (Do Nascimento et al., 2015).

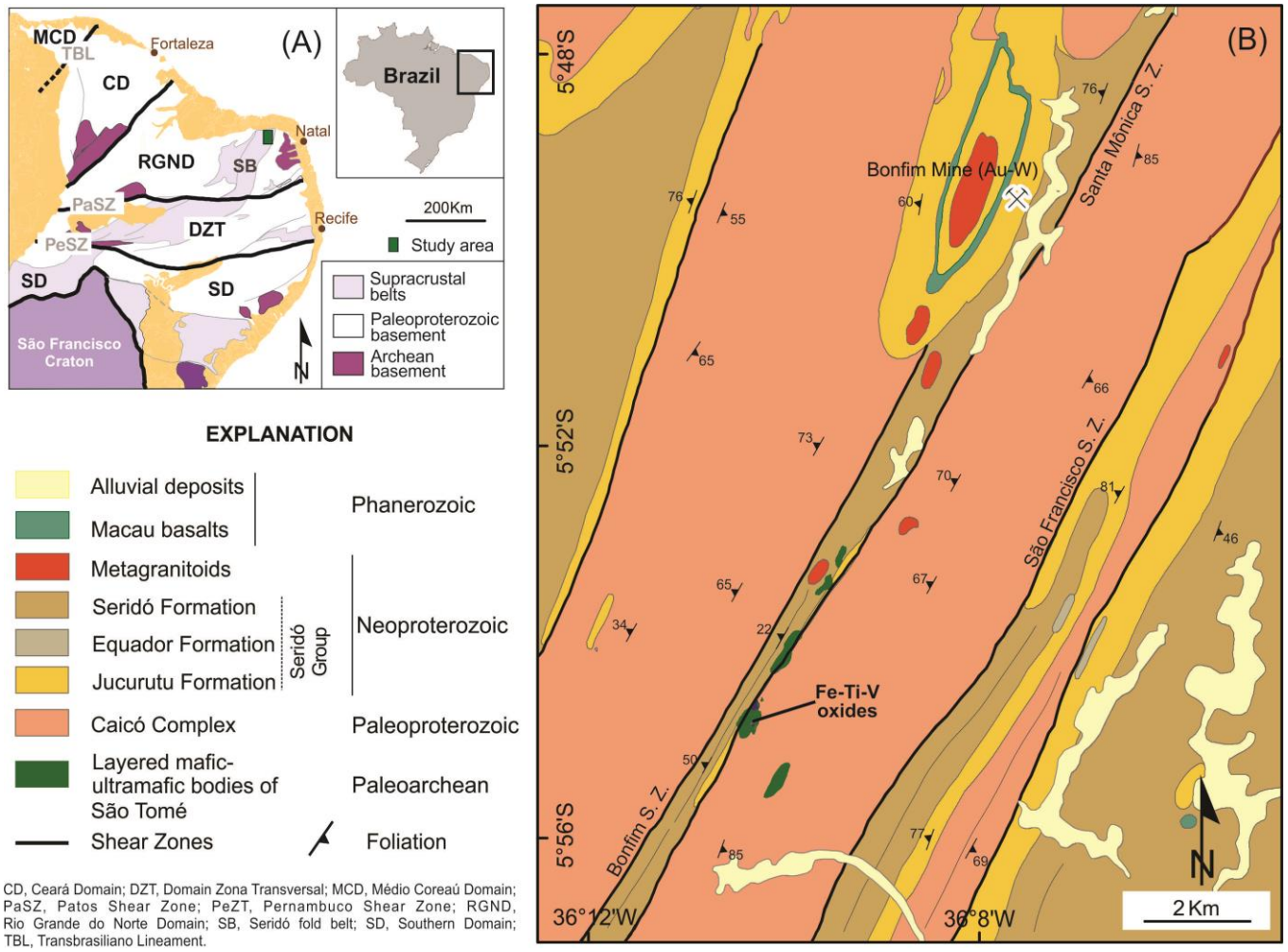

Fig. 3. (A) A simplifies geological map of the Borborema Province in northeast Brazil (modified after Van Schmus et al. 2003). (B) Local geological map to the north of the Seridó Belt, modified after (Costa & Dantas 2014) that shows the distribution of the layered mafic-ultramafic bodies of Sao Tomé.

2.2. Seridó Belt

The Seridó Belt is a Neoproterozoic NNE-trending unit located to the east of the Rio Grande do Norte Domain (Fig. 3) that limit with the São José do Campestre Massif by the Picuí-João Câmera shear zone. The Seridó Belt mainly comprises supracrustal sequences of the Seridó Group, metamorphosed in amphibole facies, which includes paragneises and marbles of the Jucurutú Formation in the base (Fig. 4), quartzites of the Equador Formation and micaschists of the Seridó Formation, to the top (De Sa et al., 1995; Van Schmus et al., 2003; Hollanda et al., 2015). This supracrustal sequence was deposited over the Paleoproterozoic garnet-bearing paragneisses, metaplutonic units and migmatites of the Caicó Complex (De

Souza et al., 2007). Similarly to the rest of the Rio Grande do Norte Domain, the Seridó belt was intruded by granitoids with a wide range of composition from syenogranite to gabbro around 635 Ma (Do Nascimento et al., 2015).

In addition to the complex kinematic field, the Seridó Belt has a large variety of mineral resources that have been explored and exploited since the 1940s discoveries of W-Au mineralized skarns of the Bonfim Mine (Fig. 3) and Currais Novos, to the north, along with Ta-Nb-rich pegmatites and gold-bearing quartz veins (Souza Neto et al., 2008). Conversely, Costa et al., (2014) began to investigate occurrences of Fe-Ti-V oxide ores in differentiated mafic-ultramafic body near the municipality of São Tomé (Figs. 3 and 4). This differentiated body was previously identified and mapped by the Geological Survey of Brazil (CPRM) in the Lajes sheet (Costa & Dantas, 2014), which increases the importance of this region as a potential exploration mining area.

3. Layered Mafic-Ultramafic Bodies of São Tomé

The layered mafic-ultramafic bodies of São Tomé is a group of metamorphosed dismembered intrusive rocks (Figs. 3 and 4) that crops out over an area of 658.000 m^2, which are embedded whiting the Santa Monica dextral shear zone, at the contact between the Seridó formation and the Caicó Complex (Costa et al., 2014). This layered intrusion has a narrow range of composition from ol-websterite to pyroxenite (Fig. 4). Meter-sized massive ilmenite-magnetite lenses are observed in the main intrusion (Fig. 4), which was selected for a comprehensive petrological and geochronological study. Five drill-cores from an extensive drilling program conducted by Eagle Star Mining Corp. in the area were systematically sampled in order to address questions regarding the evolution of the São Tomé suit as well as its metallogenetic potential.

The intrusion can be grouped into two sections (Fig. 4): (1) a ultramafic section primarily composed of Ol-websterite and pyroxenite that displays cumulate olivine bands, pyroxene, amphibole and bands of magnetite and ilmenite. Plagioclase was not observed in this section. (2) A metamorphosed section mainly composed by hornblendite with abundant amphibole, pyroxene, plagioclase and rhythmic micro-layers of magnetite and ilmenite.

The basement of the layered mafic-ultramafic bodies of São Tomé is a medium to coarse grained Mt-Ilm-bearing Hbl-Bt-Pl-Qtz orthogneiss (Fig. 5), which is characterized as having strong foliation marked by biotite and hornblende.

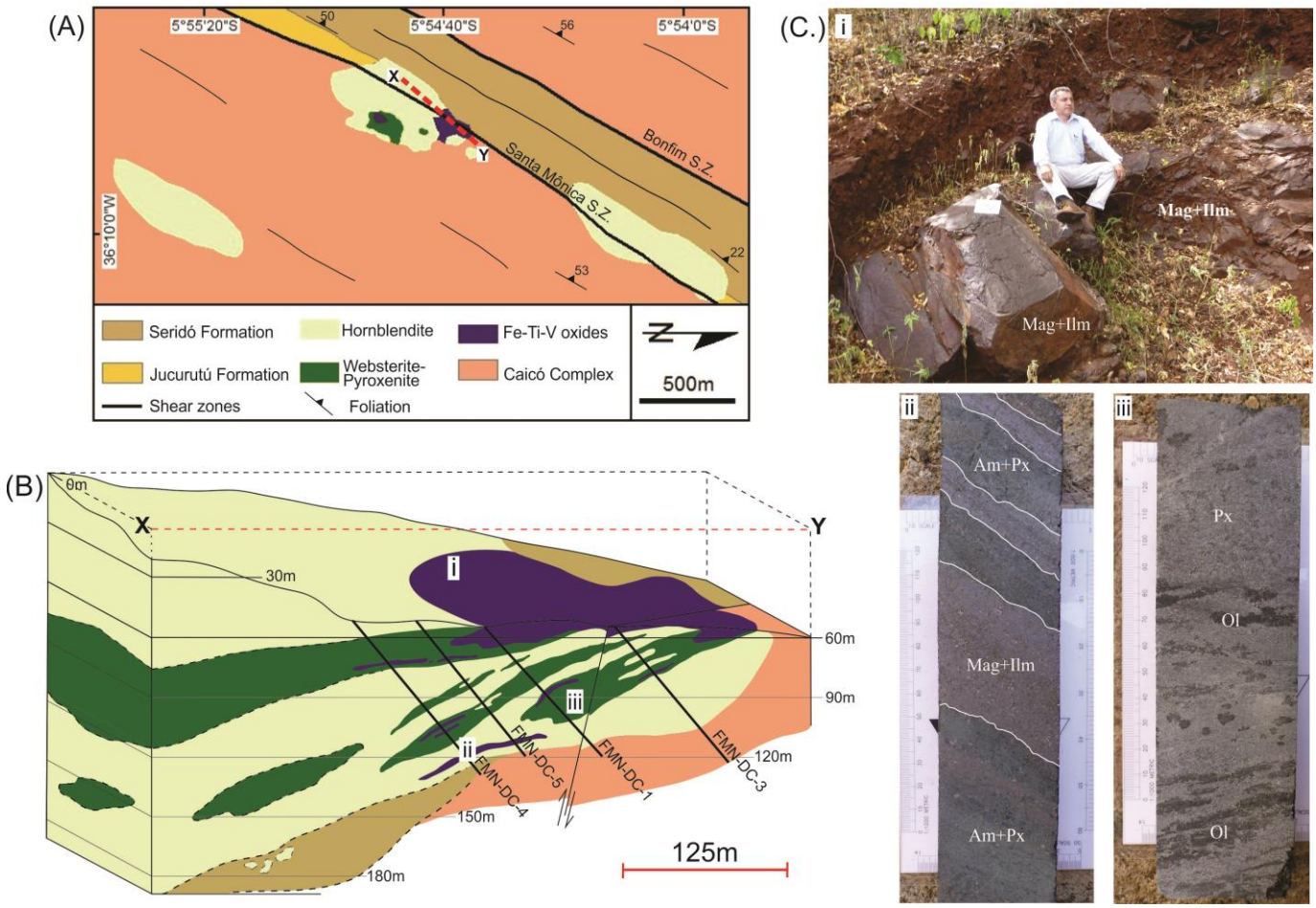

Fig. 4. (A) Simplified geological map of the larger mafic-ultramafic bodies of São Tomé, which shows the Fe-Ti-V oxide ores. (B) Geological profile of one of the bodies with its respective drilling location. (C) Outcrop and drill cores present in the geological profile: (i) Outcrop of the mineralized zone with blocks of magnetite and ilmenite. (ii) Pyroxene-hornblendite rock core showing micro rhythmic layers of magnetite and ilmenite (iii) Olivine-websterite rock core with olivine bands. Am: amphibole; Ilm: ilmenite; Mag: magnetite; Ol: olivine; Px: pyroxene.

3.1. Metamorphism and metasomatism

Metamorphism was mainly seen in the mafic section, which has banding marked by amphibole. Thus, hornblendite is the rock with greater development of foliation by its content of amphibole (> 70%) and for a Q-limit (Fig. 5), composed by plagioclase, quartz and titanite. On the other hand, metamorphism is less present in ultramafic rocks. Evidence of foliation can be observed in Ol-websterite by the distortion of the olivine bands (Fig. 5) which at the same time are rimed by serpentine. Pyroxenite shows irregular fractures through the drill cores and also a change in the tonality was observed, from light to dark green. It was possible to observe an intense process of metasomatism, characterized by the pervasive formation of dark green chlorite and tabular phlogopite without evidence of plastic crystal deformation (Fig. 5) that sharply cuts both igneous layers and metamorphic banding in pyroxenite. Moreover,

hornblendite has an alteration front that dramatically changes the green tonality of the hornblendite by an irregular yellowish green mass (Fig. 5), characterized by the formation of epidote, zoisite and pyrite (Fig. 5). There are also brownish yellow phlogopite bands 4 cm thick, cutting obliquely the igneous and metamorphic structures in pyroxenite and hornblendite (Fig. 5).

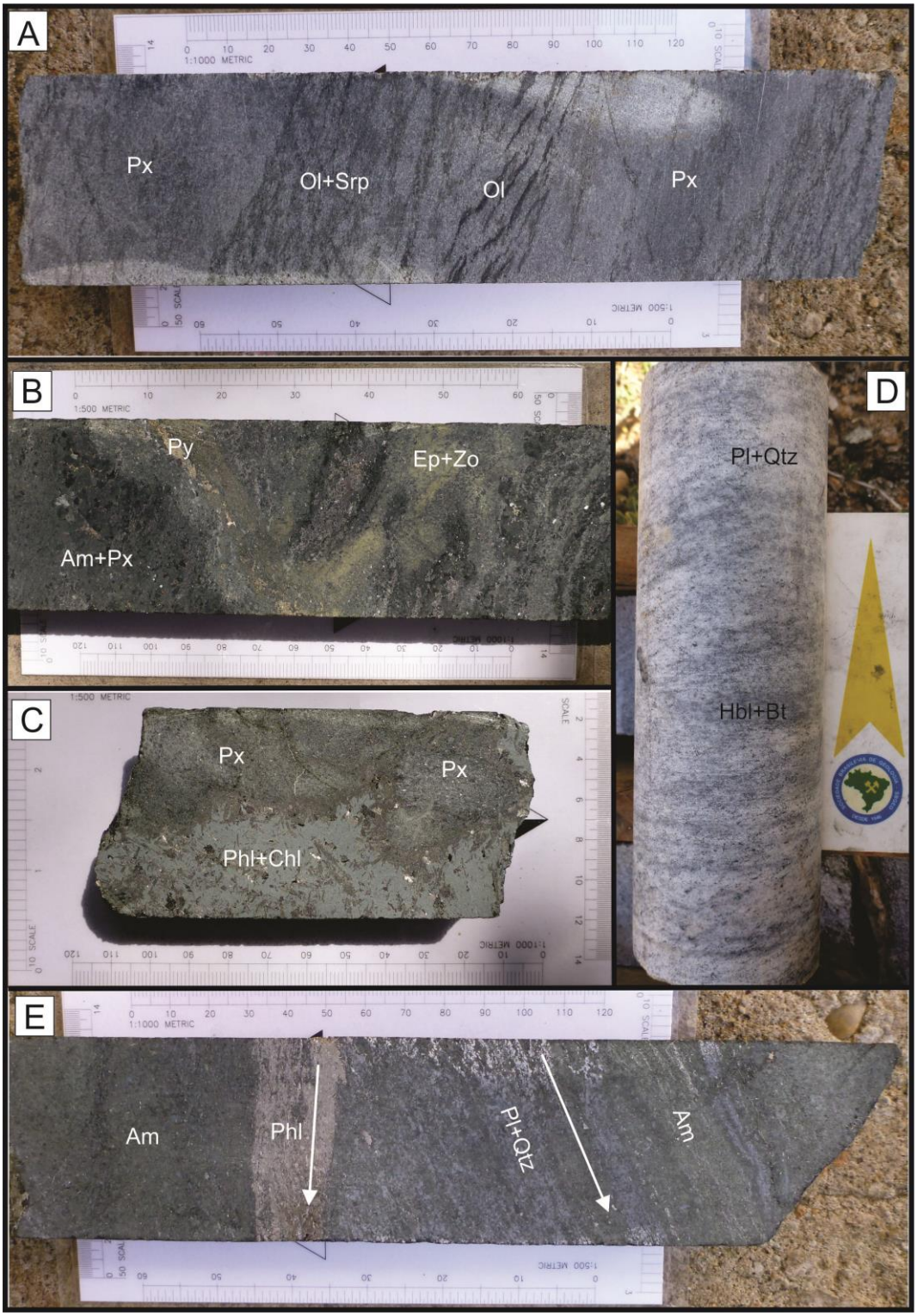

Fig. 5. Metamorphosed and metasomatized drill cores of the São Tomé Suit and its gneissic basement: (A) Hornblendite rock core showing distortion of the black olivine bands and in the brownish green olivine bands that are rimmed by serpentine. (B) Hornblendite rock core showing an alteration with formation of epidote, zoisite and pyrite. (C) Pyroxenite rock core showing a metasomatic front of phlogopite and chlorite. (D) Hbl-Bt-Pl-Qtz orthogneiss rock core showing foliation marked by hornblende and biotite. (E) Hornblendite rock core showing foliation market by amphibole and by the Q-limit which consist in quartz and plagioclase. A brownish yellow phlogopite band is cutting obliquely the foliation.

3.2. Petrography

Most of Ol-websterite are fine to coarse grained rocks, which display dark discontinuous olivine bands that are 4-15 mm thick (Fig. 4) and rimmed by serpentine. They are typically composed of the following minerals (modal percentages): 45% clinopyroxene, 30% olivine, 15% orthopyroxene, representing the essential minerals, characterized by its anhedral shapes and some areas have a grain reduction through fractures. Accessories minerals are magnetite (5%), chlorite (3%) and serpentite (2%). Clinopyroxenites are dark, fine to medium grained rocks, composed mainly of anhedral clinopyroxene (Fig. 6C) with edges in disequilibrium, 5 modal percent each of anhedral orthoamphibole and euhedral hornblende and also pyrite and pyrrotite as accessories. In contrast, some areas have secondary chlorite and phlogopite without evidence of plastic crystal deformation. Phlogopite is euhedral ranging from 1-6 mm with a decussated texture and inclusions of rounded apatite.

Hornblendites are fine to medium grained rocks, composed of the following minerals (modal percentages): 60% hornblende and 32% clinopyroxene, representing the essential minerals. Although pyroxene crystals are anhedral, hornblende is euhedral with well-preserved crystals. Hornblendite also contains 5% phlogopite, 3% plagioclase and titanite and ilmenite as accessories. Some areas in these hornblendites have epidote-zoisite nests. Some hornblendites with Q-limits show a well-developed foliation marked by euhedral tabular amphiboles and display an important increase of felsic minerals: 10% plagioclase and 5% quartz and traces of titanite located inside of the Q-limits. Quartz crystals demonstrate triple junction, characterized by their polygonal crystals (Fig. 6F). The rocks of this section have been cut by bands of 4 cm thick phlogopite with anhedral k-feldspar crystals; the phlogopite displays a decussate texture without deformation.

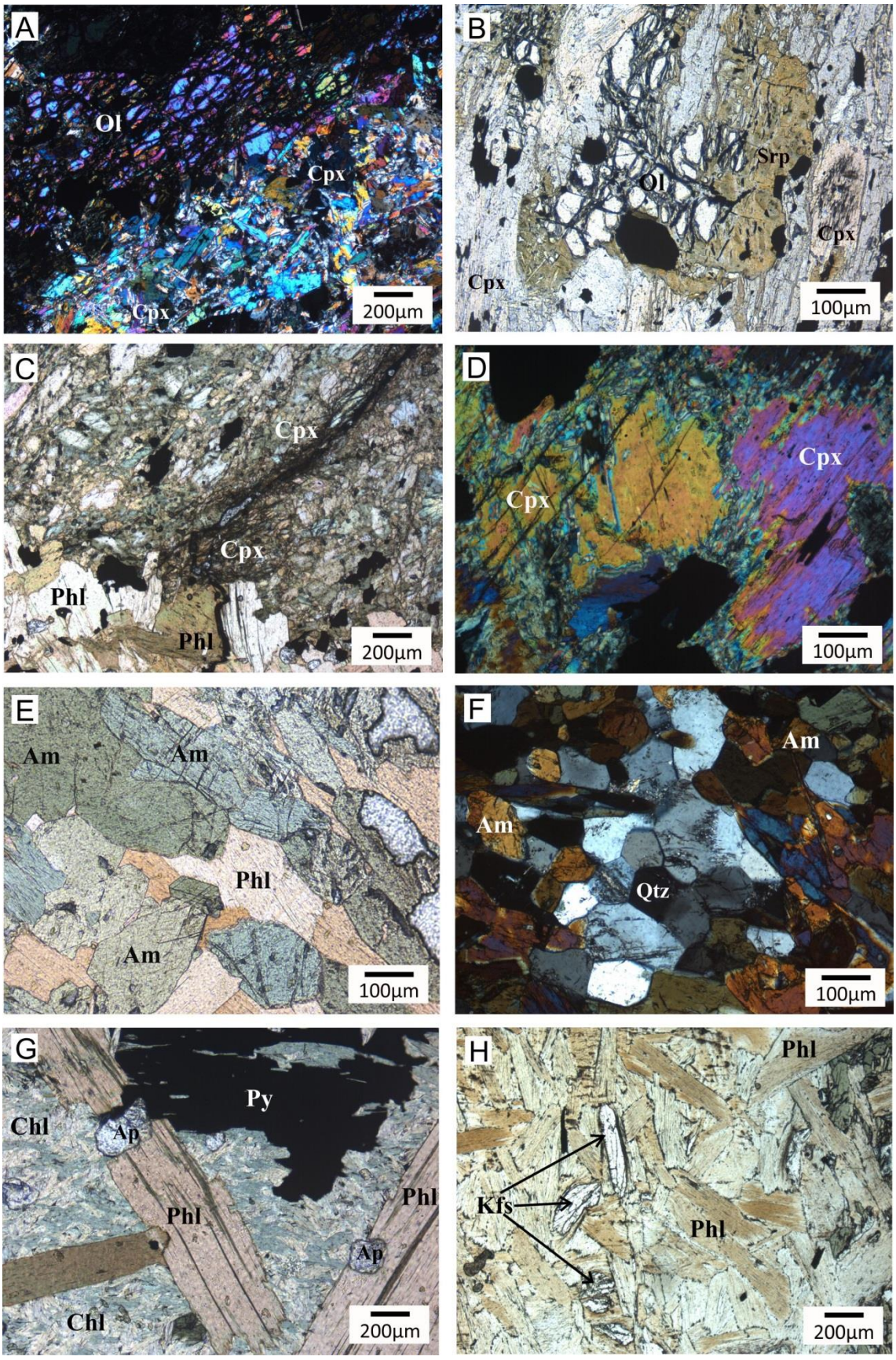

Fig. 6. Photomicrographs of samples from the differentiated mafic-ultramafic bodies of São Tomé, NE Brazil. (A) Ol-websterite primarily composed of olivine and clinopyroxene; sample

Vela-021. (B) A partially serpentinized olivine crystal in an Ol-websterite; sample Vela-008. (C) Clinopyroxenite composed of clinopyroxene, which is crossed by a layer of phlogopite; sample Vela-007. (D) Two partially altered clinopyroxenes by the edges; sample Vela-007. (E) A phlogopite bearing Hbl-pyroxenite essentially composed of euhedral amphibole, subhedral clinopyroxene and phlogopites and local orthopyroxene; sample Vela-030B. (F) Amphibole and quartz with triple junctions in metahornblendite; sample Vela-012. (G) Chlorite and phlogopite without deformation in clinopyroxenite; sample Vela-007. (H) A k-feldspar-bearing phlogopite layer without structures indicative of plastic crystal deformation, cutting a metahornblendite; sample Vela-012. (A), (D), (F) and (G) were taken under transmitted light with crossed polar lenses; (B), (C) and (E) under plane-polarized light. Am, amphibole; Chl, chlorite; Cpx, clinopyroxene; Kfs, k-feldspar; Ol, olivine; Phl, phlogopite; Qtz, quartz; Srp, serpentine.

3.3. Fe-Ti-V Ore

The layered mafic-ultramafic bodies of São Tomé have outcrops (Fig. 4) with eroded massive blocks of ~1.5 m long and ~1.0 m wide of Fe-Ti-V oxide ores. They are composed mainly by titanomagnetite and ilmenite. In general the oxide ores occur as conformable layers, being 1.2 m thick in the upper part, with more than 90% of the volume being Fe-Ti-V oxides and less than 10% volume of pyroxene and amphibole. There are also lenses of oxide ores within the Hbl-clinopyroxenite of 0.5-1 m thick that have ~55% of the volume being Fe-Ti-V oxides and ~45% volume of phlogopite widespread throughout the body. Despite the tectonism in the region (Vauchez et al., 1995), phlogopite in the lenses does not shows structures indicative of plastic crystal deformation, on the contrary it has decussated texture.

Titanomagnetite in the conformable layers is coarse grained, subhedral to euhedral (Fig. 7A) and contains ilmenite exsolution lamellae 100-600 µm long that is distributed along the cleavage planes. The oxidation in the ore layers originated hematite from magnetite, replaced towards the edges and also through the fractures. Oxidation can be observed under a microscope as the change from a dark pink to a light gray (Fig. 7b). On the other hand, ilmenite is euhedral, polygonal with several triple junctions in 120° and has weak hematite exsolution lamellae of 100-900 µm long (Fig. 7C). The oxide ores may also occur as disseminated grains in which ilmenite are rimmed by titanite in metahornblendite, some of these ilmenites have been progressively replaced entirely by titanite (Fig. 7F).

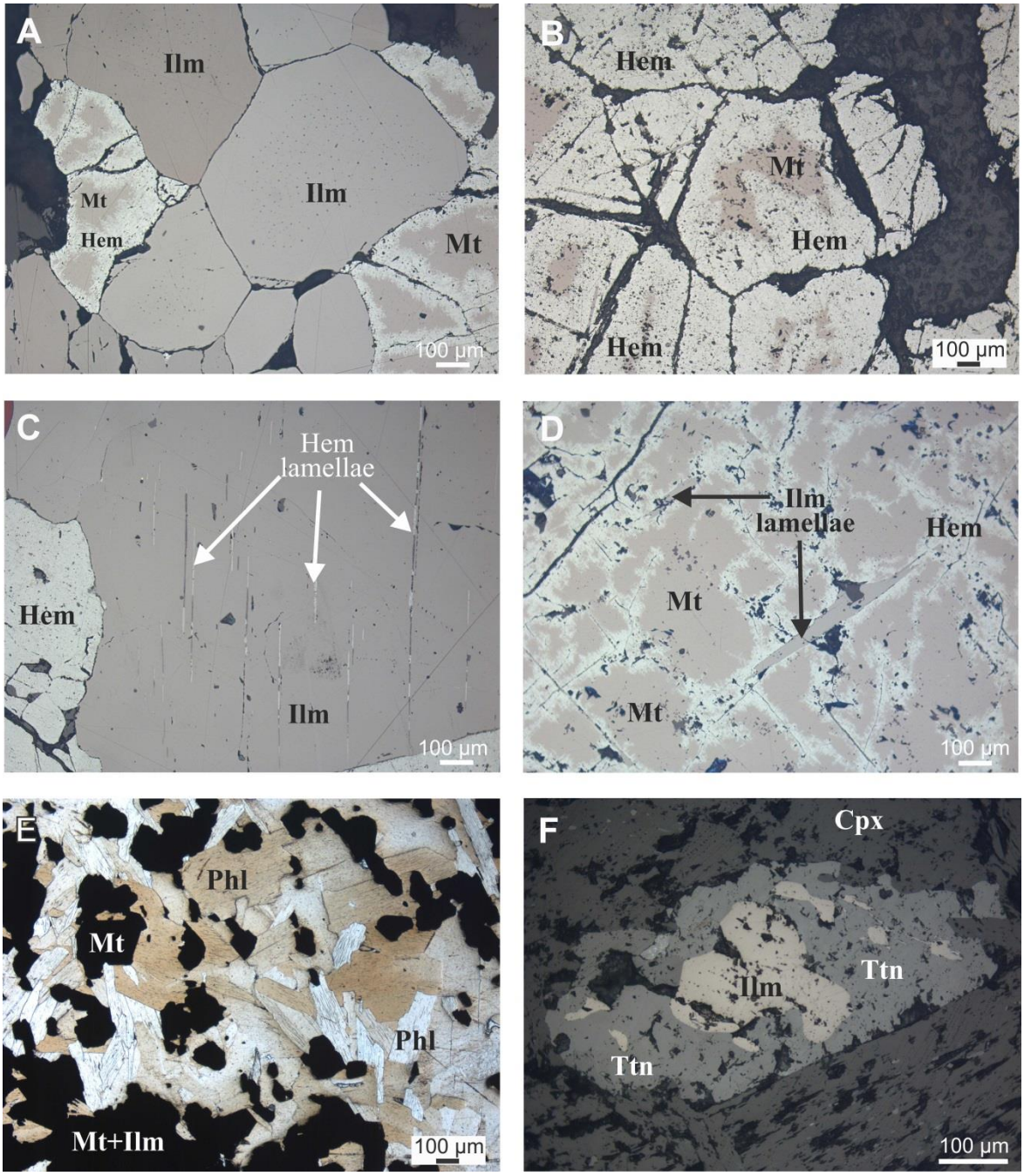

Fig. 7. Photomicrographs of the Fe-Ti-V Oxide ores. (A) Polygonal ilmenite with triple junctions and anhedral magnetite; sample Vela-003. (B) Subhedral magnetite which shows partial oxidation to hematite towards the edges; sample Vela-001. (C) Tiny light gray hematite lamellae in ilmenite; sample Vela-001 (D) Brown ilmenite lamellae in magnetite; sample Vela-003. (E) Lens of ilmenite-magnetite with decussate phlogopite that shows pleochroism of incolorous to brown; sample Vela-030B (F) A core of ilmenite rimmed by titanite in pyroxene hornblendite; sample Vela-019. (A), (B), (C) and (D) are BSE; (E) Was taken under plane-polarized light and (F) under transmitted light with crossed polar lenses. Cpx, Clinopyroxene; Hem, hematite; Ilm, ilmenite; Mt, magnetite; Phl, phlogopite; Ttn, titanite.

4. Methods

4.1. Mineral Chemistry

Electron Microprobe Analysis (EMPA) was carried out on polished thin section using a 5-spectrometer JEOL JXA-8230 SuperProbe, at the Electron Microprobe Laboratory of the University of Brasília. The wavelength dispersive (WDS) analyses were performed at an accelerating voltage of 15 kV and a beam current of 10 nA, with a counting time of 20 seconds. Synthetic and natural mineral standards patterns of oxides and silicates were used for the chemical analyses. Systematic WDS analyses of olivine, the pyroxene group, the amphibole group, phlogopite, chlorite, ilmenite and magnetite were obtained, as they are show in Tables 1-3. H_2O, Fe_2O_3, FeO, Fe^{3+} and Fe^{2+} were estimated on the stoichiometry basis of each mineral.

4.2. Sm-Nd isotopic analyses

The Sm–Nd isotopic followed the method described by (Gioia & Pimentel, 2000) at the Geochronology Laboratory of the University of Brasília. Whole-rock powders (~200 mg) were mixed with ^{149}Sm–^{150}Nd spike solution and dissolved in Savillex capsules. Sm and Nd extraction of whole-rock samples followed conventional cation exchange techniques. Sm and Nd samples were loaded on Re evaporation filaments of double filament assemblies, and the isotopic measurements were carried out on a multi-collector Finnigan Triton mass spectrometer in static mode. The $^{143}Nd/^{144}Nd$ ratios were normalized to $^{146}Nd/^{144}Nd$ of 0.7219, and the decay constant used was 6.54×10^{-12}. T_{DM} values were calculated using the DePaolo (1981) model and the results are shown in Table 6.

4.3. LA-ICP-MS U-Pb zircon analyses

Zircon crystals were obtained from 9 kg rock samples using conventional gravimetric and magnetic techniques at the Geochronology Laboratory of the University of Brasília. The crystals were chosen by handpicking using a binocular microscope. Before every micro-analytical procedure, zircon mounts were cleaned with dilute (2%) HNO_3. Backscattered electron images were obtained using a FEI-QUANTA 450 SEM working at 15 kV at the University of Brasília to record and analyze the zircon grains. For U-Pb isotopic analyses, the samples were mounted in an especially adapted laser cell and loaded into a New Wave UP213 Nd:YAG laser (λ=213nm), linked to a Thermo Finnigan Neptune Multi-collector ICPMS. The laser was run at a frequency of 10 Hz and energy of ~100mJ/cm^2 with a spot diameter of 30μm for U-Pb systematics. The isotopic analyses followed procedures described by (Bühn et al., 2009) and were carried out at the Geochronology Laboratory of the University of Brasília.

A fragment of zircon standard GJ-1 (Jackson et al., 2004) was used as the primary reference material in a standard-sample bracketing method, accounting for mass bias and drift correction (Albarède et al., 2004). An internal standard was run at the start and at the end of each analytical session, yielding accuracy around 2% and a precision in the range of 1% (1σ). Uncertainties in sample analyses were propagated by quadratic addition of the external uncertainty observed for the standards to the reproducibility and within-run precision of each unknown analysis. Zircon grains with $^{206}Pb/^{204}Pb$ lower than 1000 were rejected. Plotting of U-Pb data was performed using ISOPLOT v.3.7 (Ludwig, 2008). U-Pb results are shown in Table 6.

4.4. Oxigen fugacity

To obtain a conventional two oxide temperature and fO_2 for magnetite and ilmenite was used QUILF program of (Andersen et al. 1993; Andersen & Lindsley 1988), using the major elements obtained by EMPA (*i.e.* Al_2O3, TiO_2, Fe_2O_3, FeO, MnO and MgO) in each mineral phase, a fixed pressure of 2000 bar (selection of pressure is unimportant here because the two oxide thermometer is essentially independent of pressure, according to Andersen et al. 1993), a trial enter value of 1373 °K and by last a trial enter value of -10 fO_2.

5. Results

5.1. Mineral Chemistry

Even though feldspars, sulfides, calcite and titanite were identified in the described samples, electron microprobe analyses have focused on minerals that played an important role in the metallogenesis and subsequent re-equilibrium, such as olivine, pyroxene, amphibole, phlogopite, chlorite, magnetite and ilmenite.

5.1.1. Olivine

Most of the olivine analyses were performed on crystal cores due to the partial serpentinization in ol-websterite. The composition of olivine crystals vary in a range between $Fo_{77.83}$ to $Fo_{87.28}$, which shows high tenors of Mg (Table 1). Concentration of Ni is variable, with Ni contents between 2000 ppm to 4605 ppm (Fig. 8).

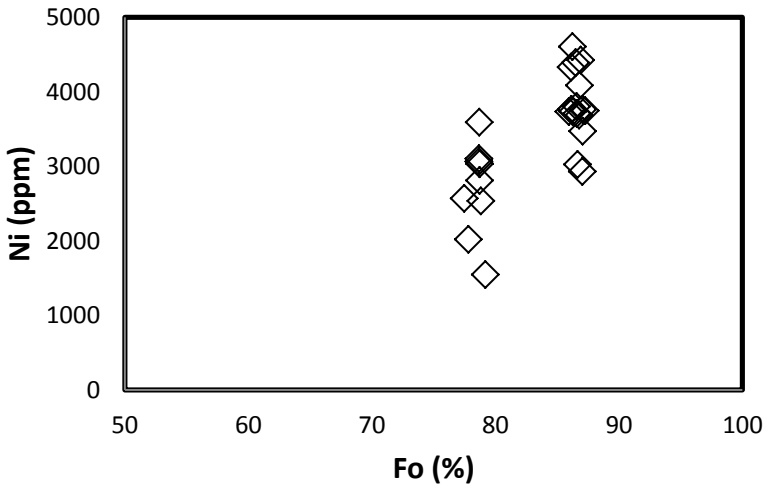

Fig. 8. Plots of Fo vs. Ni content of olivine in Ol-websterite.

5.1.2. Pyroxene Group

The pyroxene group involves cumulus crystals of augite and enstatite (Fig. 9), both are anhedral and shows reaction edges. Augite is a common phase in the ultramafic level, which has almost homogeneous composition, with SiO_2 contents of 53.35-58.38 wt.%, CaO of 12.24-12.81 wt.%, MgO of 19.18-22.59 wt.% with moderate enstatite values, ranging between $En_{59.62}$ and $En_{66.62}$. Despite of the regular composition even in rocks that lack amphibole (*i.e.*

clinopyroxenite), augite crystals display high aluminum content, with values greater than 2.0 wt.% to 5.30 wt.% (Fig. 10). Conversely, enstatite is uncommon and restricted to ol-websterite and hornblendite, with SiO_2 contents of 48.05-54.68 wt.%, CaO contents less than 1.0 wt.%, MgO of 19.10-29.03 wt.% and enstatite contents varying from $En_{59.06}$ to $En_{76.02}$ (Table 1). There is a continuous trend of Al_2O_3 enrichment that involves both enstatite and augite from Ol-websterite to clinopyroxenite (Fig. 10).

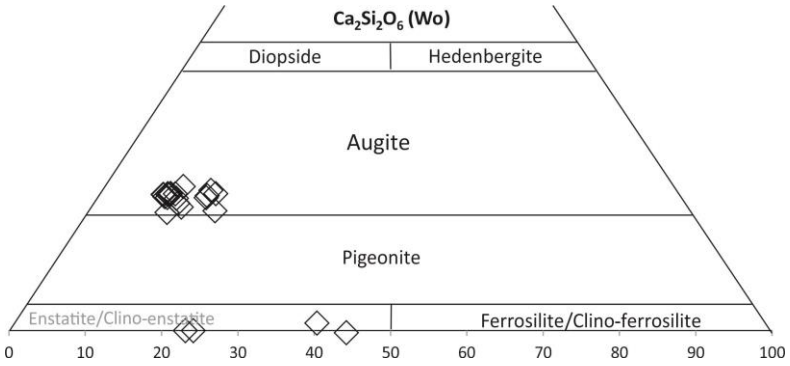

Fig. 9. Triangular diagram for the pyroxene classification showing the phases founded in the layered mafic-ultramafic bodies of São Tomé, after (Deer et al. 1986).

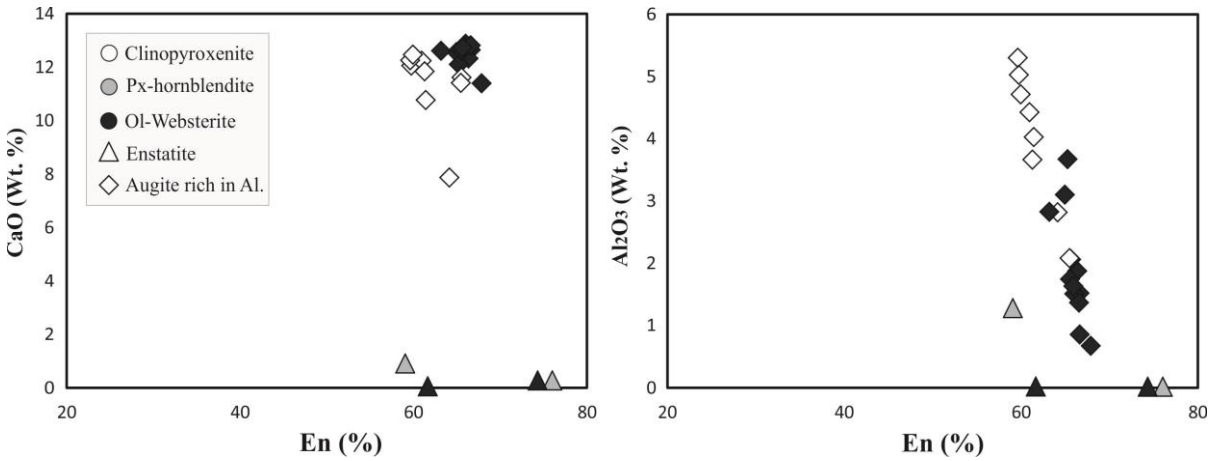

Fig. 10. Plot of En (%) vs CaO (Wt.%) and En (%) vs Al2O3 (Wt.%) content of enstatite and Al-rich augite in clinopyroxenite, Px-hornblendite and Ol-websterite.

5.1.3. Amphibole group

Amphibole is the most common constituent in the mafic level, which was formed both in igneous and metamorphic processes. This mineral group involves Mg-hornblende, tschermakite and Mg-gedrite (Figs. 11 and 12). Mg-Hornblende represents the relict of the primary igneous

phases, which was preserved only inside the Fe-Ti-V oxide layers with anhedral shapes. Mg-Hornblende has SiO_2 contents of 44.43-52.47 wt.%, CaO of 9.51-13.02 wt.% and MgO of 8.86-18.17 wt.% (Table 1), moreover, like in the pyroxene group, there is a Al_2O_3 enrichment which can be seen in a negative $Al_{(iv)}$ trend in Fig. 13. Tschermakite is the most widespread amphibole in the mafic-ultramafic bodies which together with Mg-gedrite was formed in the metamorphic stage, whereby shows orientated crystals with euhedral shapes. Tschermakite has SiO_2 contents of 42.62-44.29 wt.%, CaO of 10.72-11.31wt.%, and MgO of 9.82-11.69 wt.%. Mg-gedrite is the orthorhombic phase founded in the sample Vela-021with SiO_2 contents of 40.77-42.37 wt.%, CaO contents less than 0.07 wt.% and MgO of 31.72-32.86 wt.%.

The abundance of tschermakite and also the appearance of Mg-gedrite may be associated by a metamorphism in amphibole facies. Thus, among the amphiboles above, the increase in the replacement of $Al_{iv} \leftrightarrow Si_{iv}$ in tetrahedral site as well as the $Fe_{+3}/(Fe_{+3}+Al_{iv})$ ratio provided a great opportunity to differentiated primary igneous to metamorphic phases, as is shown in Fig. 13.

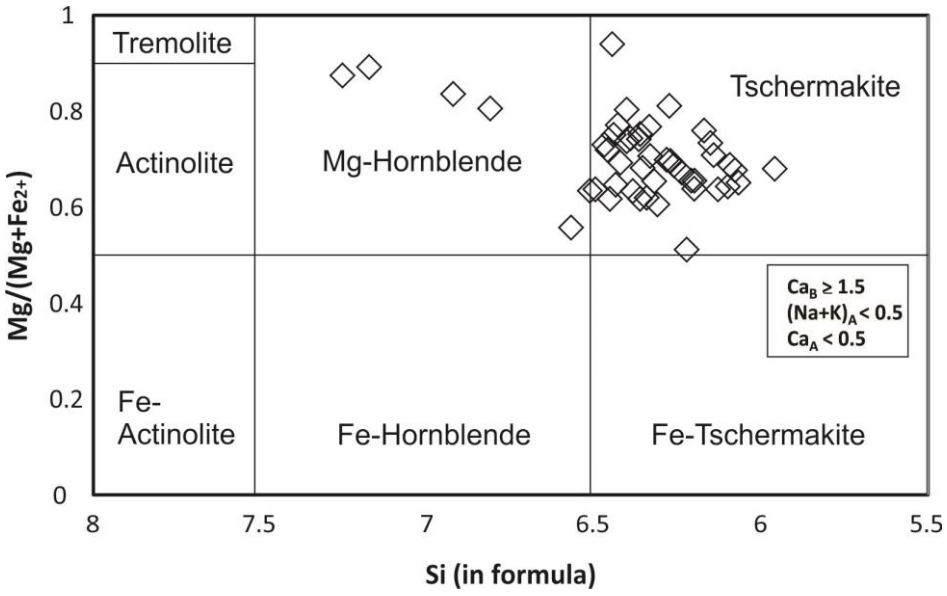

Fig. 11. Classification of the calcic amphiboles in the layered mafic-ultramafic bodies of São Tomé, showing plots falling between the tschermakite and Mg-hornblende fields, after (Leake et al. 1997).

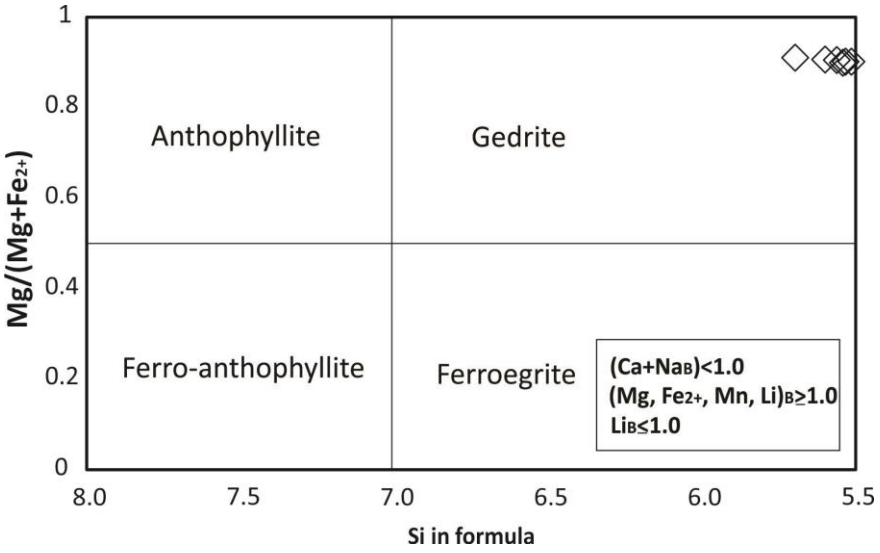

Fig. 12. Classifications for the Mg-Fe-Mn-Li amphiboles in the mafic-ultramafic bodies of São Tomé, showing plots falling in the gedrite field, after (Leake et al. 1997).

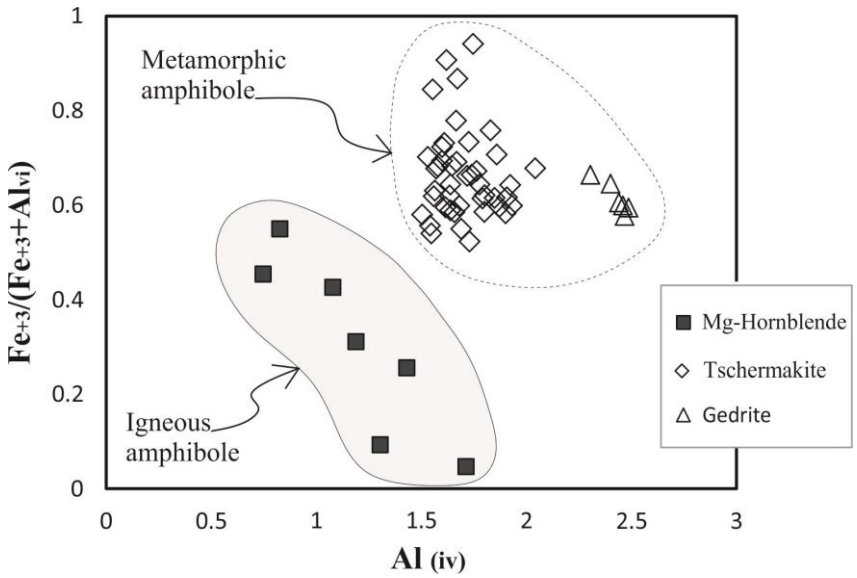

Fig. 13. Plot of $Al_{(iv)}$ vs $Fe_{+3}/(Fe_{+3}+Al_{(vi)})$ content for Mg-Hornblende, Tschermakite and Mg-Gedrite, discriminating igneous and metamorphic amphibole.

5.1.4. Phlogopite

According to the diagram proposed by (Deer et al., 1986) there are three main groups of phlogopites: (1) a group plotting between phlogopite-eastonite field, formed in the beginning of the metasomatic stage associated with chlorite, which is dark green, tabular and have inclusions of apatite. (2) A group that falls in the phlogopite field *sensu stricto*, with dark brown colors, formed inside the bands of magnetite and ilmenite. (3) And a final group that falls between the phlogopite-eastonite field with brownish yellow color, formed in bands cutting hornblendites and associated with k-feldspar.

In general phlogopite crystals are characterized to be rich in Mg, $Al_{(iv)}$ and Ti (Table 2). The Fe/(Fe+Mg) ratio never exceeds 0.5 and the groups are separated from each other by a progressively increases of Ti and Fe (Fig. 14) with maximum values of 2.87 wt.% and 18.62 wt.% respectively.

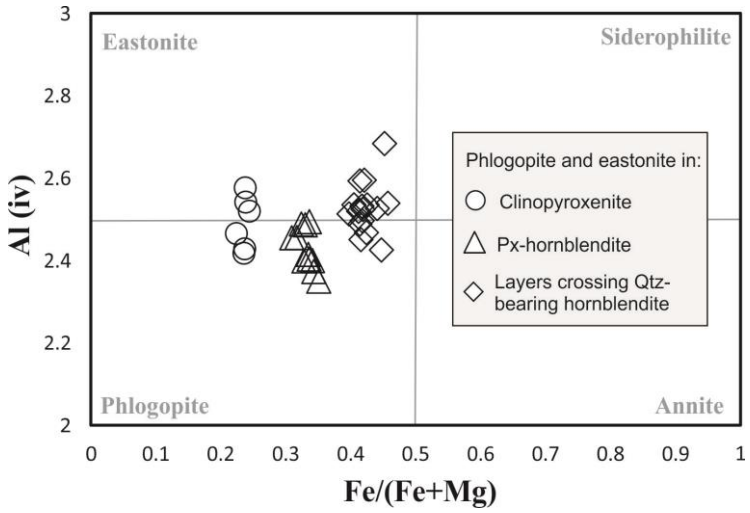

Fig. 14. Compositional variation diagram of phlogopite in clinopyroxenite, Px-hornblendite and layers crossing Qtz-bearing hornblendite in the mafic-ultramafic bodies of São Tomé. The Al(iv)-Fe/(Fe+Mg) diagram (after Deer et al. 1986) shows an intermediate composition between phlogopite and eastonite.

5.1.5. Chlorite

There are two groups of chlorites as it shows in the Si vs. Fe/(Fe+Mg) diagram after Hey, (1954). One group rich in Mg derived from Ol-websterite and clinopyroxenite, that falls in the chlinoclore and sheridanite fields (Fig. 15), with MgO contents of 25.61-32.54 wt.% and moderated contents of FeO of 5.74-11.52wt.%. The second group is rich in Fe derived from hornblendites, falling between the ripidolite and brunsvigite fields, with MgO contents of 7.05-

8.32 wt.% and FeO of 36.00-37.27wt.% (Table 2). Both groups have low contents of CaO and MnO (Table 2). Previous data suggest that the protolith is decisive in the replacement of Fe ↔Mg for the chemical composition of chlorites.

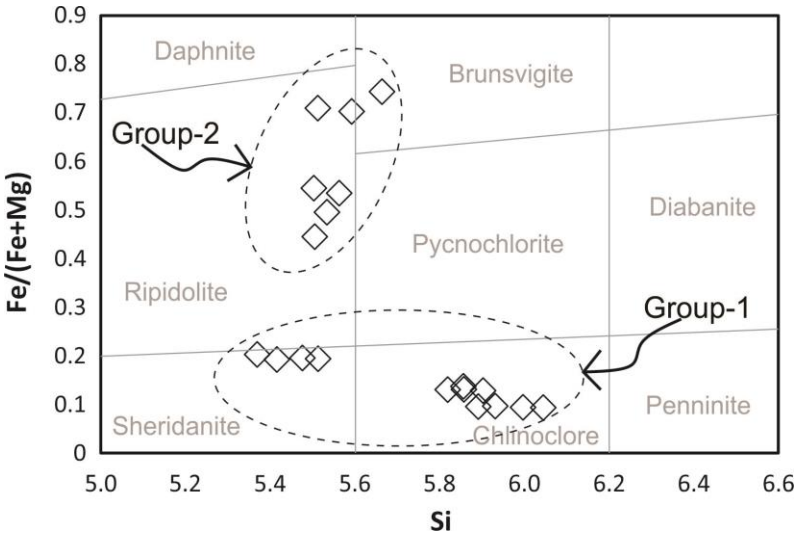

Fig. 15. Nomenclature and classification of chlorite in the mafic-ultramafic bodies of São Tomé, after (Hey 1954).

5.1.6. Compositions of Magnetite and Ilmenite

Titanomagnetite is the richest mineral phase in vanadium, with V_2O_3 contents of 1.38-1.98 wt.%, with a flat distribution and no significant changes in oxidation by the pass to hematite (Fig. 16) while vanadium is absent in basement magnetite. Titanomagnetite displays a negative increasing distribution for $FeO_{(total)}$ (91.44-99.46 wt.%) and TiO_2 (0-4.18 wt.%) attributed to magmatic differentiation that is distorted by hematite plots which display iron loss (Fig. 16). Basement magnetite is almost 100 wt.% $FeO_{(total)}$, with some significant traces of SiO_2 and TiO_2 (Table 3). Thus, electron microprobe analysis of titanomagnetite and basement magnetite, indicate that because of their chemistry, both are not correlated.

Table 1. Selected electron microprobe analysis of primary igneous and metamorphic minerals in the mafic-ultramafic bodies of São Tomé.

	Primary igneous phases												Metamorphic phases				
Mineral	Olivine			Augite			Enstatite			Hornblende			Tschermakite			Gedrite	
Samp. No.	Vela-021-5	Vela-029-1	Vela-029-2	Vela-007-1	Vela-021-1	Vela-021-3	Vela-030B-1	Vela-030B-2	Vela-008 - 5	Vela-002-1	Vela-017B-1	Vela-006-3	Vela-006-1	Vela-012-2	Vela-030B-2	Vela-021-2	Vela-021-5
Rock code	Owb	Owb	Owb	Cpxt	Owb	Owb	Phbl	Phbl	Owb	Clfe	Hblt	Hblt	Hblt	Hblt	Phbl	Owb	Owb
SiO_2	38.79	39.66	40.23	54.27	57.55	58.39	54.68	54.05	49.39	52.47	44.43	45.11	42.62	42.97	44.29	41.41	41.37
TiO_2	0.00	0.03	0.08	0.13	0.23	0.12	0.00	0.19	0.00	0.29	0.63	0.49	0.87	0.78	0.56	0.00	0.04
Al_2O_3	0.00	0.00	0.01	4.42	1.37	0.85	1.28	0.02	0.02	6.81	11.35	14.68	13.08	12.84	12.24	18.23	18.90
Cr_2O_3	0.00	0.00	0.01	0.01	0.00	0.08	0.00	0.00	0.03	0.08	0.00	0.00	0.02	0.04	0.07	0.21	0.26
FeO	20.27	11.87	12.68	6.65	3.71	3.53	21.56	16.15	24.87	7.57	16.39	16.00	17.84	18.08	16.25	6.75	6.94
MnO	0.27	0.23	0.30	0.30	0.01	0.09	0.57	0.35	0.53	0.11	0.21	0.24	0.19	0.27	0.22	0.00	0.00
MgO	40.44	46.56	45.66	19.88	22.54	22.52	19.10	29.03	22.12	18.17	11.35	8.86	10.41	9.82	11.69	32.34	31.81
CaO	0.00	0.00	0.00	12.24	12.80	12.81	0.91	0.27	0.06	13.02	12.18	9.51	10.94	11.23	10.72	0.01	0.07
Na_2O	0.02	0.00	0.00	0.66	0.30	0.06	0.48	0.00	0.04	0.54	1.64	1.54	1.64	1.63	1.56	0.00	0.00
K_2O	0.00	0.01	0.01	0.09	0.02	0.01	0.11	0.00	0.00	0.08	0.36	2.48	0.41	0.41	0.24	0.05	0.02
NiO	0.26	0.48	0.59	0.12	0.07	0.07	0.07	0.07	0.47	0.00	0.00	0.05	0.06	0.00	0.09	0.11	0.12
Total	99.85	100.06	100.20	98.79	98.60	98.53	98.77	100.11	97.52	99.14	98.53	98.96	98.06	98.06	97.92	99.09	99.54
4 oxygen				6 oxygen						23 oxygen							
Si	1.00	1.00	1.01	Si	1.96	2.00	2.00	2.00	1.96	1.94	Si	7.25	6.51	6.57	6.26	6.34	6.42	5.56	5.53
Fe(ii)	0.44	0.25	0.26	Al (iv)	0.04	0.00	0.00	0.00	0.00	0.00	Al (iv)	0.75	1.49	1.43	1.74	1.66	1.58	2.44	2.47
Mn	0.01	0.00	0.01	Al(vi)	0.15	0.11	0.11	0.11	0.00	0.00	Al (vi)	0.36	0.47	1.08	0.52	0.58	0.52	0.44	0.51
Mg	1.55	1.74	1.70	Fe(iii)	0.00	0.00	0.00	0.00	0.10	0.18	Ti	0.03	0.07	0.05	0.10	0.09	0.06	0.00	0.00
Ni	0.01	0.01	0.01	Fe(ii)	0.20	0.11	0.11	0.69	0.37	0.61	Fe(iii)	0.30	0.52	0.38	1.05	0.81	1.09	0.68	0.70
Sum	3.00	3.00	2.99	Mn	0.01	0.00	0.00	0.02	0.01	0.02	Fe(ii)	0.55	1.43	1.52	1.03	1.33	0.76	0.00	0.00
Fo	77.83	87.28	86.24	Mg	1.07	1.20	1.19	1.07	1.57	1.30	Mg	3.74	2.48	1.92	2.28	2.16	2.53	6.47	6.34
Fa	21.88	12.48	13.43	Ca	0.47	0.49	0.49	0.04	0.01	0.00	Ca	1.93	1.91	1.48	1.72	1.78	1.67	0.00	0.01
Ni (ppm)	2020	3748	4605	Sum_cat	4.00	4.00	4.00	4.00	4.00	4.00	Na	0.15	0.46	0.44	0.47	0.47	0.44	0.00	0.00
				Wo	26.97	27.17	27.23	2.02	0.52	0.12	K	0.01	0.07	0.46	0.08	0.08	0.04	0.01	0.00
				En	60.96	66.56	66.62	59.05	76.02	61.66	OH	1.99	1.99	1.99	1.98	1.99	1.99	2.00	2.00
				Fs	12.07	6.27	6.15	38.93	23.47	38.22	Sum. Cat.	17.09	17.45	17.38	17.26	17.32	17.16	17.65	17.61
				WEF	100	100	100	100	100	100	$Fe_{+3}/(Fe_{+3}+Al_{vi})$	0.45	0.52	0.26	0.67	0.58	0.68	0.61	0.58

Rock code: Clfe- comformable layers of Fe-Ti-V; Cpxt-Clinopyroxenite; Hblt-Hornblendite; Owb-Ol-Websterite; Phbl- Px-hornblendite.

Table 2. Selected electron microprobe analysis of hydrothermal phlogopite and clorite in the mafic-ultramafic bodies of São Tomé.

	Phlogopite									Chlorite					
Rock type	Clinopyroxenite			Px-hornblendite			Layers of phlogopite crossing hornblendite			Ol-websterite and Clinopyroxenite			Hornblendite		
Sample	Vela-007-2	Vela-007-3	Vela-007-5	Vela-030A-1	Vela-030A-2	Vela-030B	Vela-012-2	Vela-006-1	Vela-024-1	Vela-008-1	Vela-008-2	Vela-007-2	Vela-017B-1	Vela-017B-2	Vela-017B-3
SiO_2	37.34	38.41	38.75	37.61	37.57	38.27	37.28	35.82	36.09	32.03	31.12	27.42	26.36	25.04	25.92
TiO_2	0.82	0.75	0.83	1.18	1.29	1.27	2.51	2.87	1.42	0.00	0.00	0.14	0.33	0.14	0.10
Al_2O_3	17.72	17.62	17.54	17.93	17.97	16.23	16.07	16.56	16.43	17.31	17.62	22.42	19.86	19.12	18.90
FeO	10.94	10.03	10.44	14.05	14.41	15.16	18.62	18.14	18.19	5.87	5.76	11.51	36.00	36.10	37.27
MnO	0.13	0.09	0.03	0.07	0.02	0.14	0.01	0.14	0.06	0.00	0.03	0.17	0.20	0.22	0.29
MgO	19.23	19.24	18.77	15.87	15.77	15.61	12.77	13.88	13.92	32.19	32.07	25.61	8.32	8.28	7.05
CaO	0.11	0.04	0.00	0.00	0.02	0.01	0.00	0.05	0.00	0.04	0.04	0.00	0.13	0.13	0.13
Na_2O	0.69	0.70	0.51	0.76	0.69	0.26	0.43	0.46	0.20	0.00	0.00	0.03	0.05	0.01	0.00
K_2O	8.66	8.61	8.97	8.09	7.91	8.67	8.40	7.11	8.71	0.05	0.02	0.00	0.00	0.00	0.00
F	0.00	0.03	0.00	0.05	0.02	0.00	0.13	0.07	0.00	0.00	0.00	0.00	0.04	0.01	0.05
Cl	0.11	0.03	0.03	0.04	0.04	0.04	0.05	0.02	0.06	0.01	0.00	0.02	0.00	0.00	0.02
NiO	0.04	0.10	0.09	0.09	0.00	0.07	0.00	0.07	0.03	0.25	0.16	0.14	0.00	0.00	0.00
H2O*	4.13	4.16	4.16	4.09	4.09	4.06	4.01	3.99	3.96	12.70	12.56	12.23	11.21	10.88	10.87
Total	99.93	99.78	100.05	99.93	99.99	99.92	100.77	99.21	99.19	100.83	99.71	99.74	102.76	100.02	100.77
22 oxygen										*36 oxygen*					
Si	5.42	5.53	5.57	5.51	5.51	5.65	5.57	5.41	5.48	6.04	5.93	5.37	5.59	5.51	5.66
Al (iv)	2.58	2.47	2.43	2.49	2.49	2.35	2.43	2.59	2.52	1.96	2.07	2.63	2.41	2.49	2.34
Al (vi)	0.46	0.53	0.54	0.61	0.61	0.47	0.40	0.35	0.41	1.90	1.90	2.55	2.58	2.48	2.55
Ti	0.09	0.08	0.09	0.13	0.14	0.14	0.28	0.33	0.16	0.00	0.00	0.02	0.05	0.02	0.02
Fe	1.30	1.20	1.25	1.71	1.75	1.86	2.30	2.21	2.27	0.93	0.97	1.90	6.21	6.62	6.64
Mg	4.16	4.13	4.02	3.47	3.45	3.44	2.84	3.12	3.15	9.06	9.11	7.48	2.63	2.72	2.30
Na	0.19	0.19	0.14	0.22	0.20	0.07	0.13	0.13	0.06	0.00	0.00	0.02	0.04	0.01	0.00
K	1.61	1.58	1.64	1.51	1.48	1.63	1.60	1.37	1.69	0.02	0.01	0.00	0.00	0.00	0.00
OH*	3.97	3.98	3.99	3.97	3.98	3.99	3.93	3.96	3.99	15.99	16.00	15.99	15.94	15.99	15.92
Sum. Cat	19.78	19.69	19.69	19.61	19.60	19.60	19.49	19.47	19.72	36.01	36.08	36.03	35.78	35.96	35.77

Similar to magnetite, ore ilmenite display a negative increasing distribution of $FeO_{(total)}$ (34.22-51.68 wt.%) and TiO_2 (37.88-54.47 wt.%) (Fig. 16), and also a restricted field for V_2O_3 (0.43-0.78 wt.%) and MgO (0.023-2.74 wt.%). Ilmenite exsolution lamellae is depleted in $FeO_{(total)}$ (41.38-44.09 wt.%) but enriched in TiO_2 (52.59-53.92 wt.%) (Table 4). Basement ilmenite is depleted in V_2O_3 (0.28-0.46 wt.%), impoverished in MgO (0.00-0.05 wt.%) but shows high content of MnO with values up to 1.78 wt%.

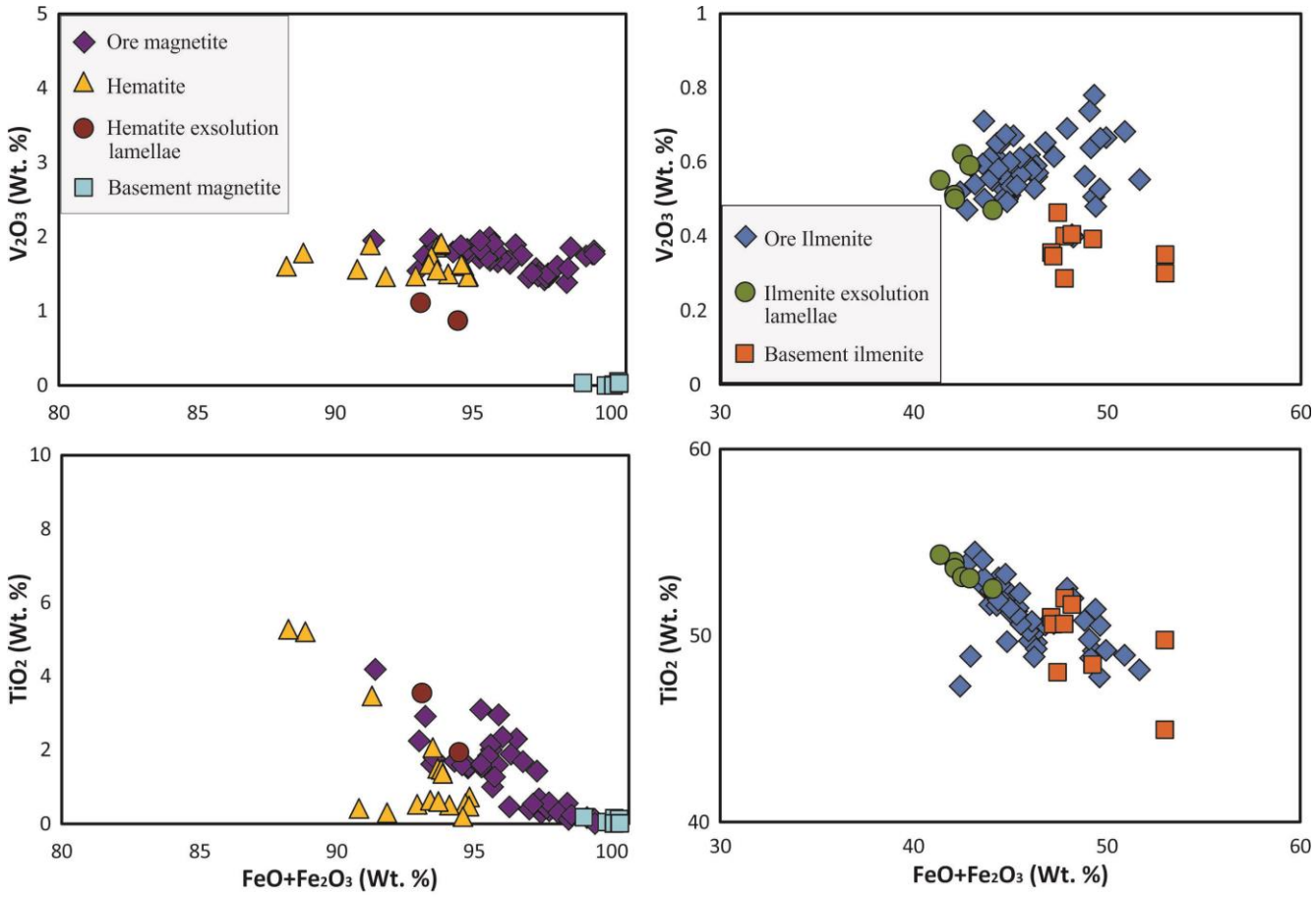

Fig. 16. Plots of $FeO+Fe_2O_3$ (wt.%) vs. TiO_2 (wt.%) and $FeO+Fe_2O_3$ (wt.%) vs. V_2O_3 (wt.%) for titanomagnetite and ilmenite in ore layers and the basement.

In order to complement the analysis for the ore assemblage, we use QUILF program (Andersen and Lindsley, 1988; Andersen et al., 1993; Ghiorso and Sack, 1991), with which titanomagnetite and ilmenite shows an oxygen fugacity between -17.9 to -22.8 fO_2 and temperatures between 500°C to 576°C as shows Fig. 17. Inclusions of ilmenite and hematite not were included in the analyses due to the high content of TiO_2 in hematite, which may be attributed to the interaction between the inclusion and the host mineral at the moment of the microanalyses.

Table 3. Selected electron microprobe analysis of magnetite in the mafic-ultramafic bodies of São Tomé and its basement.

Mineral	Ore magnetite				Basement magnetite				Hematite (oxidation)				Hematite exsolution lamellae	
Sample	Vela-001	Vela-001	Vela-001	Vela-001	Vela-013	Vela-013	Vela-013	Vela-013	Vela-001	Vela-001	Vela-001	Vela-001	Vela-001	Vela-001
SiO_2	0.100	0.016	0.050	0.053	0.000	0.208	0.070	0.067	0.170	0.240	0.170	0.130	0.080	0.130
TiO_2	0.390	1.836	1.532	1.603	0.041	0.175	0.000	0.011	1.500	1.470	1.360	2.060	3.540	1.930
NiO	0.040	0.038	0.034	0.055	0.000	0.000	0.076	0.000	0.090	0.020	0.070	0.040	0.010	0.000
Al_2O_3	0.680	0.465	0.578	0.410	0.075	0.008	0.000	0.018	0.550	0.690	0.530	0.730	0.620	0.590
Fe_2O_3	65.715	62.964	63.161	62.981	68.802	67.748	69.087	69.036	61.903	61.787	62.077	61.110	59.953	62.258
FeO	31.356	32.611	32.161	32.326	31.082	31.302	31.061	31.115	31.816	32.061	31.830	32.431	33.202	32.247
MnO	0.000	0.000	0.052	0.026	0.000	0.000	0.000	0.083	0.052	0.095	0.000	0.124	0.080	0.000
MgO	0.160	0.151	0.244	0.145	0.000	0.000	0.052	0.000	0.160	0.130	0.130	0.170	0.630	0.170
V_2O_3	1.450	1.714	1.827	1.946	0.000	0.034	0.009	0.000	1.860	1.890	1.910	1.740	1.110	0.870
Cr_2O_3	0.050	0.263	0.221	0.255	0.000	0.082	0.017	0.016	0.010	0.050	0.120	0.080	0.060	0.000
Total	99.962	100.079	99.860	99.820	100.000	99.598	100.400	100.394	98.112	98.453	98.197	98.614	99.374	98.255

Table 4. Selected electron microprobe analysis of ilmenite in the mafic-ultramafic bodies of São Tomé and its basement.

Mineral	Ore Ilmenite					Ilmenite exsolution lamellae					Basament ilmenite			
Sample	Vela-001	Vela-001	Vela-001	Vela-001	Vela-001	Vela-001	Vela-001	Vela-001	Vela-001	Vela-002	Vela-013	Vela-013	Vela-013	Vela-013
SiO_2	0.010	0.030	0.021	0.034	0.012	0.010	0.070	0.020	0.080	0.010	0.025	0.025	0.024	0.059
TiO_2	51.410	51.470	50.743	50.588	51.217	53.920	54.320	53.590	52.490	53.120	44.946	44.946	48.443	50.607
NiO	0.010	0.000	0.000	0.058	0.053	0.010	0.030	0.000	0.000	0.000	0.022	0.022	0.000	0.000
Al_2O_3	0.010	0.050	0.051	0.061	0.052	0.010	0.770	0.040	0.050	0.000	0.000	0.000	0.007	0.004
Fe_2O_3	3.300	2.912	3.925	4.832	3.874	0.000	0.000	0.000	1.646	0.000	14.248	14.248	7.606	3.425
FeO	41.930	42.499	42.196	40.724	41.163	42.120	41.380	42.150	42.449	42.530	38.745	38.745	41.645	43.784
MnO	0.530	0.814	0.769	0.522	0.665	0.526	0.711	0.639	0.360	0.039	1.616	1.616	1.783	1.781
MgO	2.130	1.680	1.510	2.434	2.414	1.970	2.120	2.120	2.500	1.650	0.049	0.049	0.055	0.000
V_2O_3	0.570	0.580	0.578	0.564	0.534	0.510	0.550	0.500	0.470	0.620	0.300	0.300	0.392	0.346
Cr_2O_3	0.010	0.000	0.000	0.000	0.087	0.010	0.000	0.000	0.000	0.030	0.000	0.000	0.000	0.000
Total	99.911	100.036	99.793	99.817	100.071	99.086	99.951	99.059	100.045	97.999	99.951	99.951	99.956	100.006

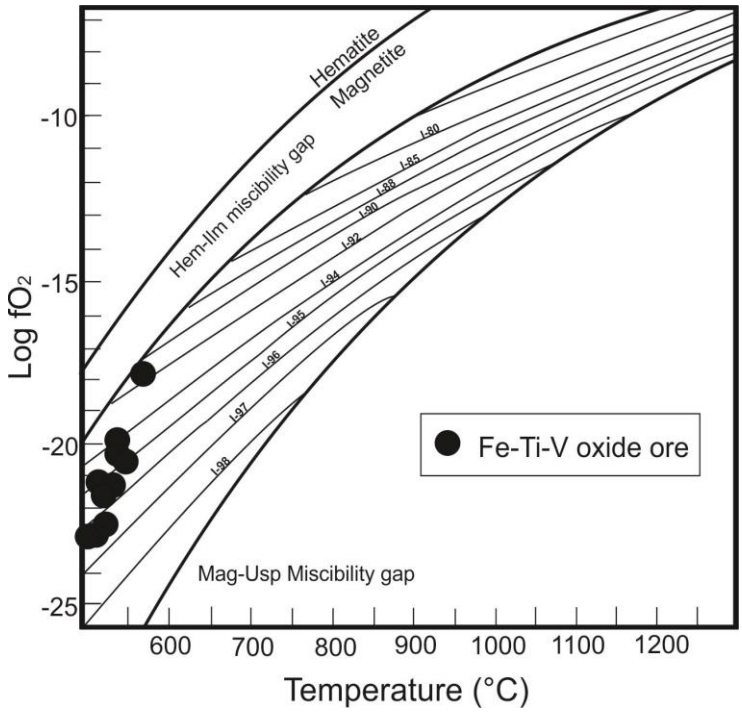

Fig. 17. Log fO_2 – Temperature diagram constructed from compositions of coexisting magnetite and ilmenite in the layered mafic-ultramafic bodies of São Tomé. Log fO2 and temperature were calculate using QUILF program, after (Andersen et al. 1993).

5.2. LA-ICP-MS Zircon Analytical Results

For U-Pb dating, zircons grains of Hbl-pyroxenite (sample Vela-027) and Mt-Ilm-bearing Hbl-Bt-Pl-Qtz orthogneiss (sample Vela-013) were analyzed. Zircons grains from sample Vela-027 are anhedral, highly fractured with sharp edges, and 90 by 90µm to 220 by 190µm in size (Fig. 10). Most zircons are unzoned and some have micro inclusions of quartz which were observed in BSE. On the other hand, zircon grains from sample Vela-013 are subhedral to anhedral, 70 by 140µm to 170 by 120µm in size, are less fractured and shows a relic of oscillatory zoning texture, similarly described in Harley et al., (2007).

Isotopic measurements for Hbl-pyroxenite and the gneissic basement are presented in Table 5. For sample Vela-027 nine points were measured on nine zircons and from which a Th/U ratio between 0.230 and 0.445 was obtained. Isotopic results are concordant, giving an age of 3506 ± 20 Ma (MSWD = 2.5). Sample Vela-027 have Th/U values greater than 0.1, data which is typically recognized in the magmatic field (Rubatto, 2002), therefore, based on the characteristics of the zircon grains, as well as the Th/U ratios, 3.5 Ga is interpreted as the crystallization age for the mafic-ultramafic bodies. For sample Vela-013, 28 points on 28 zircons were analyzed from which a Th/U ratio between 0.109 and 0.373 (Table 5) was obtained. In contrast to sample Vela-027, data from sample Vela-013 is discordant, giving an upper-intercept

age of 3508 ± 16 Ma (Fig. 10) and a lower-intercept age of 649 ± 56 Ma (MSWD = 4.2). Analogous to Sample-027, basement displays Th/U values greater than 0.1, which added on the characteristics of zircon grains, 3.5 Ga is interpreted as the crystallization age for the basement and 649 Ma is interpreted as the age of the Brasiliano metamorphism, which similar with ages reported for (Hollanda et al., 2015) in zircons from Jucurutú and Seridó formations.

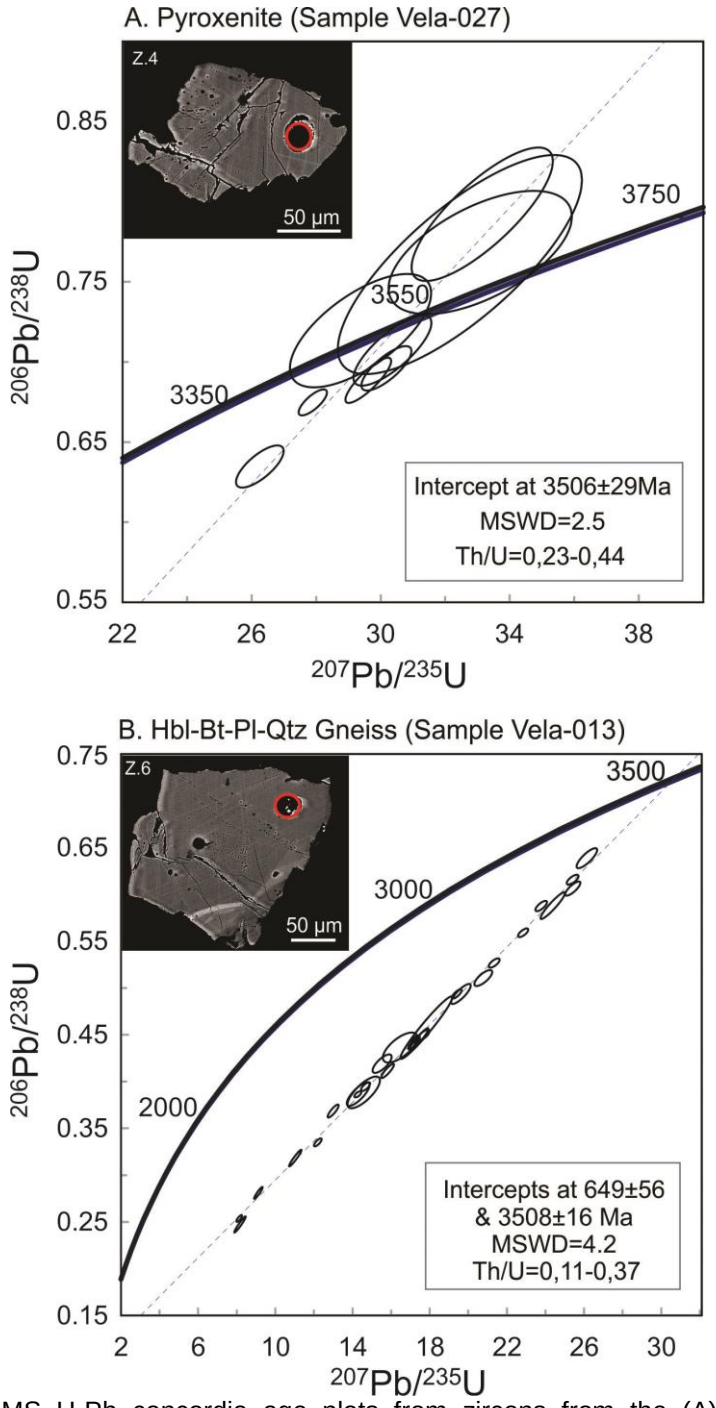

Fig. 18. LA-ICP-MS U-Pb concordia age plots from zircons from the (A) medium-grained Pyroxenite (sample Vela-027); and (B) coarse-grained Mt-Ilm-bearing Hbl-Bt-Pl-Qtz gneiss (orthogneissic basement, sample Vela-013).

Table 5. Zircon U-Pb dating results of Hbl-Piroxenite and Mt-Ilm-bearing Hbl-Bt-Pl-Qtz gneiss (basement).

Sample	Th/U	Measured isotopic ratios							Corrected ages (Ma)					
		$^{207}Pb/^{206}Pb$	1σ %	$^{207}Pb/^{235}U$	1σ %	$^{206}Pb/^{238}U$	1σ %	Rho	$^{207}Pb/^{206}Pb$	2σ	$^{207}Pb/^{235}U$	2σ	$^{206}Pb/^{238}U$	2σ
Vela-027 medium-grained Hbl-Piroxenite														
ZirR1	0.240	0.31194	0.7282	29.6169	1.5800	0.6885	1.3523	0.86	3530.6	11.2	3474.2	15.4	3377.1	35.5
ZirR2	0.230	0.30346	2.6164	33.1481	4.3609	0.7922	3.4691	0.80	3488.0	39.9	3585.0	42.1	3761.1	98.1
ZirR3	0.358	0.29608	3.6781	29.3764	4.9192	0.7195	3.2453	0.66	3449.8	55.9	3466.2	47.2	3494.3	87.0
ZirR4	0.345	0.31444	1.0082	30.1786	1.6976	0.6960	1.3146	0.77	3542.8	15.4	3492.6	16.5	3405.6	34.7
ZirR5	0.279	0.29982	0.5610	27.8966	1.0398	0.6748	0.7932	0.76	3469.3	8.7	3415.5	10.1	3324.2	20.6
ZirR6	0.250	0.29996	1.2021	26.2545	1.8577	0.6348	1.3670	0.74	3470.0	18.5	3356.1	18.0	3168.4	34.1
ZirR7	0.328	0.31139	1.5996	30.3653	2.6285	0.7072	2.0525	0.78	3527.8	24.5	3498.7	25.5	3447.9	54.6
ZirR8	0.279	0.31229	4.5918	33.0864	5.6688	0.7683	3.3034	0.58	3532.3	69.1	3583.2	54.4	3674.7	91.9
ZirR9	0.445	0.30938	4.8900	32.4563	7.6956	0.7608	5.9306	0.77	3517.8	73.5	3564.2	73.1	3647.2	163.1
Vela-013 coarse-grained Mt-Ilm-bearing Hbl-Bt-Pl-Qtz gneiss (basement)														
ZirR1	0.285	0.28522	0.0020	17.687	1.14	0.4497	0.81	0.71	3392	22	2394	32	2973	22
ZirR2	0.278	0.29391	0.0015	21.343	0.87	0.5266	0.61	0.70	3438	15	2727	27	3154	17
ZirR3	0.233	0.30408	0.0015	25.416	1.02	0.6062	0.82	0.80	3491	15	3055	40	3324	20
ZirR4	0.178	0.29515	0.0026	20.779	1.47	0.5106	1.10	0.75	3445	28	2659	48	3128	28
ZirR5	0.234	0.29641	0.0011	22.845	0.76	0.5589	0.54	0.71	3452	12	2862	25	3220	15
ZirR6	0.161	0.23240	0.0014	8.129	1.18	0.2537	0.94	0.80	3069	19	1457	25	2246	21
ZirR7	0.268	0.29353	0.0012	23.779	0.83	0.5875	0.62	0.74	3436	13	2979	29	3259	16
ZirR8	0.342	0.28126	0.0015	17.269	0.85	0.4453	0.54	0.64	3370	17	2374	22	2950	16
ZirR9	0.125	0.26798	0.0014	14.274	0.84	0.3863	0.55	0.66	3294	16	2106	20	2768	16
ZirR10	0.113	0.27893	0.0014	15.821	1.38	0.4114	1.22	0.89	3357	16	2221	46	2866	26
ZirR11	0.255	0.25145	0.0011	11.034	1.93	0.3182	1.85	0.96	3194	13	1781	57	2526	36
ZirR12	0.163	0.23536	0.0010	9.121	1.60	0.2810	1.50	0.94	3089	14	1597	42	2350	29

Sample	Th/U	Measured isotopic ratios							Corrected ages (Ma)					
		$^{207}Pb/^{206}Pb$	1σ %	$^{207}Pb/^{235}U$	1σ %	$^{206}Pb/^{238}U$	1σ %	Rho	$^{207}Pb/^{206}Pb$	2σ	$^{207}Pb/^{235}U$	2σ	$^{206}Pb/^{238}U$	2σ
ZirR13	0.156	0.23958	0.0013	8.171	2.41	0.2473	2.31	0.96	3117	17	1425	59	2250	43
ZirR14	0.169	0.28253	0.0034	17.828	4.98	0.4576	4.82	0.97	3377	38	2429	193	2981	94
ZirR15	0.286	0.29929	0.0013	25.409	0.79	0.6157	0.56	0.71	3467	13	3093	28	3324	15
ZirR16	0.150	0.26978	0.0017	14.678	1.06	0.3946	0.77	0.73	3305	19	2144	28	2795	20
ZirR17	0.240	0.25582	0.0016	12.998	1.45	0.3685	1.25	0.86	3221	20	2022	43	2680	27
ZirR18	0.195	0.28415	0.0015	17.449	1.84	0.4453	1.73	0.94	3386	16	2374	68	2960	35
ZirR19	0.176	0.28514	0.0011	19.408	0.85	0.4936	0.65	0.77	3391	12	2586	28	3062	16
ZirR20	0.246	0.30071	0.0015	24.378	1.72	0.5879	1.60	0.93	3474	15	2981	76	3284	33
ZirR21	0.173	0.28283	0.0016	17.183	1.15	0.4406	0.93	0.81	3379	18	2353	37	2945	22
ZirR22	0.373	0.29692	0.0020	26.147	1.35	0.6386	1.11	0.82	3454	21	3184	55	3352	26
ZirR23	0.132	0.28825	0.0025	19.619	1.72	0.4936	1.43	0.83	3408	27	2586	61	3073	33
ZirR24	0.107	0.26417	0.0015	12.203	1.08	0.3350	0.84	0.77	3272	18	1863	27	2620	20
ZirR25	0.183	0.26883	0.0037	15.535	2.10	0.4191	1.55	0.74	3299	42	2256	59	2849	40
ZirR26	0.109	0.26823	0.0044	14.296	2.73	0.3865	2.14	0.79	3296	51	2107	77	2770	51
ZirR27	0.381	0.27370	0.0071	16.467	3.58	0.4363	2.43	0.68	3327	81	2334	95	2904	67
ZirR28	0.328	0.27230	0.0067	14.583	3.80	0.3884	2.88	0.76	3319	76	2115	103	2788	71

5.3. Sm-Nd Analyses

Early eoarchean values were found in the layered mafic-ultramafic bodies of São Tomé with an Nd model age between 4.01 and 3,52, a ξNd(t) value between −0.14 and -2.47 and a ξNd(0) value of −4.01 and -6.83 (Table 5). Sample Vela-006 and Vela-012 gave inconsistente results probably because they were representative of metamorphism and metasomatism, thus were not taken into account, The basement has an Nd model age of 3.68 Ga and a ξNd(0) of -17.67, which shows a late eoarchean magma and a high amount of crustal contamination. Previous results contrast with the 3.4 Ga gneisses of São José do Campestre located 50 km from the layered mafic-ultramafic intrusion obtained by (Dantas et al., 2004) whose data show a similar T_{DM} but with greater crustal contamination, and an ξNd(0) reaching up to -38.7.

Table 6. Sm–Nd data for samples of the mafic-ultramafic bodies of São Tomé, its basement and the São José do Campestre massif (Dantas et al. 2004).

Sample	Rock type	Sm (ppm)	Nd (ppm)	$^{147}Sm/^{144}Nd$	$^{143}Nd/^{144}Nd$ (±2σ)	ξNd (0)	ξNd (t)	TDM (Ga)
São Tomé Intrusion (t=3.5 Ga)								
Vela-014	Pyroxenite	2.313	7.433	0.1881	0.512432±13	-4.01	-0.14	4.01
Vela-006	Hornblendite	5.354	17.763	0.182	0.512203±19	-8.49	-1.86	4.52
Vela-008	Ol-websterite	1.198	3.857	0.187	0.512288±22	-6.83	-2.47	3.57
Vela- 012	Hornblendite	5.678	17.771	0.193	0.512330±8	-6.01	-4.38	4.08
Basemen (t=3.5 Ga)								
Vela-013	*Mt-Ilm-bearing Hbl-Bt-Pl-Qtz gneiss*	35.151	134.668	0.1578	0.511732±13	-17.67	-0.10	3.68
Bom Jesus Tonalite gneiss (t = 3.45 Ga) (Dantas et al. 2004)								
ED-57	Tonalite	7.11	34.62	0.12423	0.510890 ± 10	−34.1	-1.86	3.77
ED-57F	Tonalite	5.52	25.27	0.1322	0.510961 ± 05	−32.7	-4.04	3.98
ED-57H	Amphibolite	3.71	18.45	0.1218	0.510664 ± 08	−38.7	-5.21	4.02
EC-69A	Tonalite	6.31	25.12	0.1478	0.511435 ± 20	−23.5	-1.71	3.82

7. Discussion

7.1. Magma source

Is well known that layered mafic intrusions are formed in any tectonic environment where basaltic magma is generated, and they must occur within the continental crust, what will later be exposed at the surface by erosion (Winter, 2001). Furthermore, layered mafic intrusions with Fe-Ti oxides are formed specifically from ferrobasaltic or ferropicritic magmas rich in Ti (Liu et al., 2015; Zhou et al., 2005), generated by partial melting of peridotitic mantle, that occur between the spinel lherzolite and garnet lherzolite fields (Wyllie, 1992; Best, 2003). The availability of elements such as titanium or vanadium will depend on the fertility of the mantle.

Different works that involve the genesis of layered Fe-Ti oxide ores, especially those studied in The Bushveld Complex, Sept Iles layered intrusion or the Emeishan igneous province, give three explanations for the formation of these Fe-Ti rich magmas (Charlier et al., 2015; Liu et al., 2015; Vantongeren and Mathez, 2012; Zhou et al., 2005): (1) the Fe-Ti enrichment may be the final feature of an intense differentiation process from basaltic liquids. (2) By an assimilation process between a basaltic liquid and continental rocks with high iron and titanium content, such as Banded Iron Formation. (3) From immiscible liquids rich in Fe-Ti-V±(P).

The Layered mafic-ultramafic bodies of São Tomé reports an ξNd (t) of -0.14 and -2.47 (Table 5), so that in 3.5 Ga the São Tomé bodies did not have a significant contamination, excluding the possibility of an assimilation process. The layers include cumulate olivine bands with a tenor of Fo_{87} and 4605 p.p.m. Ni (Table 3). This is a high Mg and Ni content for a differentiated rock which does not show assimilation, indicating high temperatures and pressures in the partial melting of peridotitic source (Herzberg et al., 2016). Geochemical models has been performed for basaltic magmas from peridotite sources, where the partial melting of a fertile peridotite with 1,960 p.p.m. Ni, generated olivine with tenors between 2,800 and 3,100 p.p.m Ni (Herzberg et al., 2013). Thus, due to the high content of Fo and values up to 4605 p.p.m. Ni, in addition to a high geothermal gradient in the early Archean (Martin, 1986), is assumed a fertile peridotite source in the São Tomé bodies, which in a partial melting process generated a ferropicritic or ferrobasaltic magma.

7.2. Genesis of Fe-Ti-V ores

The main factors that control the formation of Fe-Ti-V oxides are: (1) source rock or magma composition, (2) temperature, (3) pressure, (4) cooling rate, (5) oxygen fugacity fO_2 (6) sulfur fugacity, (7) silicon and sulfide activity (Nadoll et al., 2014; Pang et al., 2008).

At first, the Layered mafic-ultramafic bodies of São Tomé show a differentiation process, which forms layers of cumulate olivine and pyroxene with intercumulate hornblende while plagioclase is absent. The continuous trend of Al_2O_3 enrichment from Ol-websterite to clinopiroxenite seen on pyroxenes (Fig. 10) and the $Al_{(iv)}$ enrichment in amphiboles (Fig. 13) indicate a continuous process of fractional crystallization generating a residual liquid rich in aluminium and silica in the magmatic chamber which could trigger liquid-liquid immiscibility during differentiation, however, the presence of hydrated phases indicates a magmatic chamber rich in volatiles which according to experimental analyses on liquid immiscibility carry out by (Charlier & Grove, 2012; Hou et al., 2017; Lester et al., 2013), inhibits the formation of plagioclase and reduce the binodal curve. It means that the Fe-Ti-V ores were generated from a process of fractional crystallization and a poorly developed immiscibility as shown in Fig. 19.

It is important to analyze the high content of vanadium in magnetite, with tenors up to 1.8 wt.% V_2O_3 (Table 4). Vanadium is a compatible element in magnetite (Nadoll et al., 2014; Rollinson, 1993), and is present in this mineral as V^{3+} (Balan et al., 2006). A high vanadium content means low oxygen fugacity, because with high fO_2 values, vanadium has a valence of 5+, making it incompatible within the magnetite structure (Toplis & Corgne 2002). In addition to that, experimental results of immiscibility in basaltic liquids, showed that high values of fO_2 promotes an early crystallization of magnetite (Charlier and Grove, 2012). The above can be seen reflected in the rock with intercumulate magnetite, however, magnetite in the bodies of São Tomé are mostly presented in cumulated layers. The oxygen fugacity obtained in the ore assemblage titanomagnetite-ilmenite using QUILF Program (Andersen et al., 1993), with values ranging between -17.9 to -22.8 fO_2 (Fig. 17), explain a high content of vanadium and the absence of intercumulate magnetite due to the very low values of fO_2. Therefore, is viable the hypothesis of fractional crystallization and immiscibility at 3.5 Ga, from a fertile peridotite source (Fig. 20).

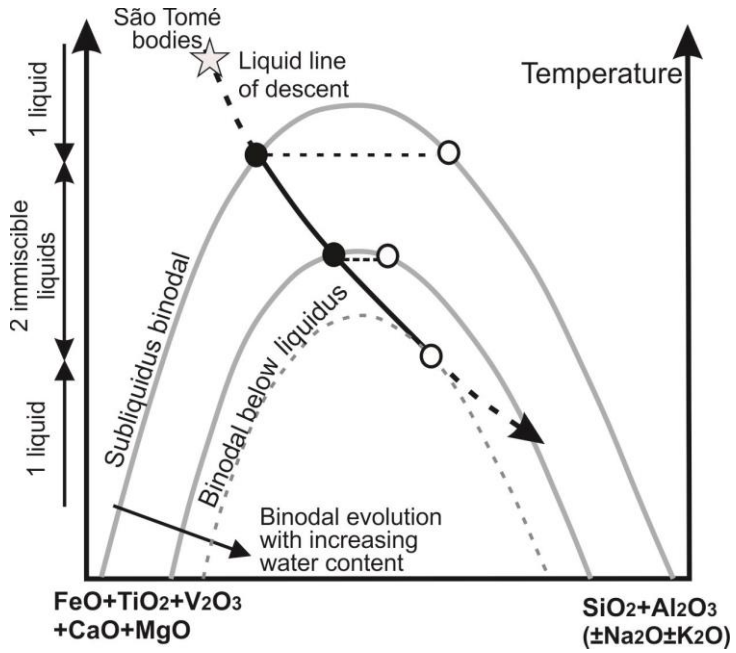

Fig. 19. Schematic illustration of the evolution of the liquid line of descent through a two liquid field, applied for the case of the layered mafic-ultramafic bodies of São Tomé, showing the effect of increasing water content during differentiation. Modifier afer (Charlier & Grove 2012).

7.3. Metamorphism and metasomatism

After the magmatic-ore stage, the layered mafic-ultramafic bodies of São Tomé underwent an intense metamorphism due to the amalgamation of Archean terrains to the supercontinent Atlantica at 2.2 Ga (Neves, 2003; Neves, 2011), and subsequently by the establishment of the Seridó Belt at 0.6 Ga (de Sa et al., 1995; Van Schmus et al., 2003), which has metamorphosed both the host rocks (Hollanda et al., 2011) and the mafic-ultramafic bodies in Amphibolite Facies, during which hornblende and pyroxene were transformed into a more stable amphibole, forming foliated and euhedral crystals of tschermakite and Mg-gedrite as well as quartz (Fig. 6F) and plagioclase. Otherwise, while mafic and ultramafic rocks had a ductile response to deformation, ore minerals had a fragile response rather than ductile, it can be observe in the structure of magnetite and ilmenite which shows a set of fractures through the ore layers. Perhaps, oxidation in magnetite began at this stage due to the particular characteristics of a hydrated metamorphism, responsible for the massive martitization.

The metamorphic stage was followed by three metasomatic stages (Fig. 20). Metasomatism began with a K-P-H_2O stage that forms two groups of phlogopites with inclusions of apatite and chlorite. Subsequently formed a Ca-Na stage, which forms epidote group minerals and sulfides plus titanite and calcite, and a final K-rich stage, that forms phlogopite bands with microcline (Fig. 6H), with content up to 2 wt.% TiO_2.

Models of experimental mineralogy, have shown that high TiO_2 contents in biotite indicate high temperatures (Henry et al., 2005; Chambers & Kohn, 2012), and also, according to the geobarometer proposed by (Henry et al., 2005), phlogopite founded in the São Tomé bodies (Table 2) can reach 700°C. Thus, phlogopite rich in Ti and also associated with k-feldspar (Wones and Eugster, 1965), indicate high temperatures, that may be sufficient to remobilize elements that generally are considered immobile such as Ti. The above was observed in the mineral chemistry of magnetite, hematite and ilmenite, in which TiO_2 and $FeO_{(Total)}$ shows variations in a negative trend. Only V_2O_3 plots remained fixed. Another evidence for the mobility of elements in the ore body is housed in the Ti (ppm) vs. Ni/Cr diagram proposed by Dare et al., (2014), in which titanomagnetite display plots between igneous and hydrothermal fields (Fig. 21), it can be explain at first by the igneous origin of titanomagnetite, that subsequently undergoes an intense metamorphism and metasomatism, remobilizing Fe, Ti, Ni and Cr while vanadium remained immobile.

7.4. Fe-Ti-V ores of São Tomé in the context of others mineralized layered mafic intrusions

Layered mafic intrusions have great economic importance due to their high content in platinum group elements, chromite, ilmenite and magnetite (Table 7). These intrusions were generated massively in Neoarquean and Meso-proterozoic (Cawthorn, 1996; Charlier et al., 2015), usually generated from mantle plumes emplaced in the continental crust. This is the case of the Bushveld Complex and the Emeishan large igneous province (Hatton, 1995; Liu et al., 2015; Zhou et al., 2005), which were highly differentiated with sequences from dunite to anortosite. In the final stage of differentiation occur the immiscibility in these deposits, generated layers of anortosite and layers of Fe-Ti oxide ores. Similarly, the layered mafic-ultramafic bodies of São Tomé generated its Fe-Ti-V oxide layers by immiscibility, but do so without developing layers of silica-aluminum-rich rocks as anortosite. Thus, the São Tomé oxide ores reached its immiscibility earlier than other similar deposits in the world (Table 7), this is a singular feature that added to its old age, differentiate the occurrence of this ores with other deposits around the world.

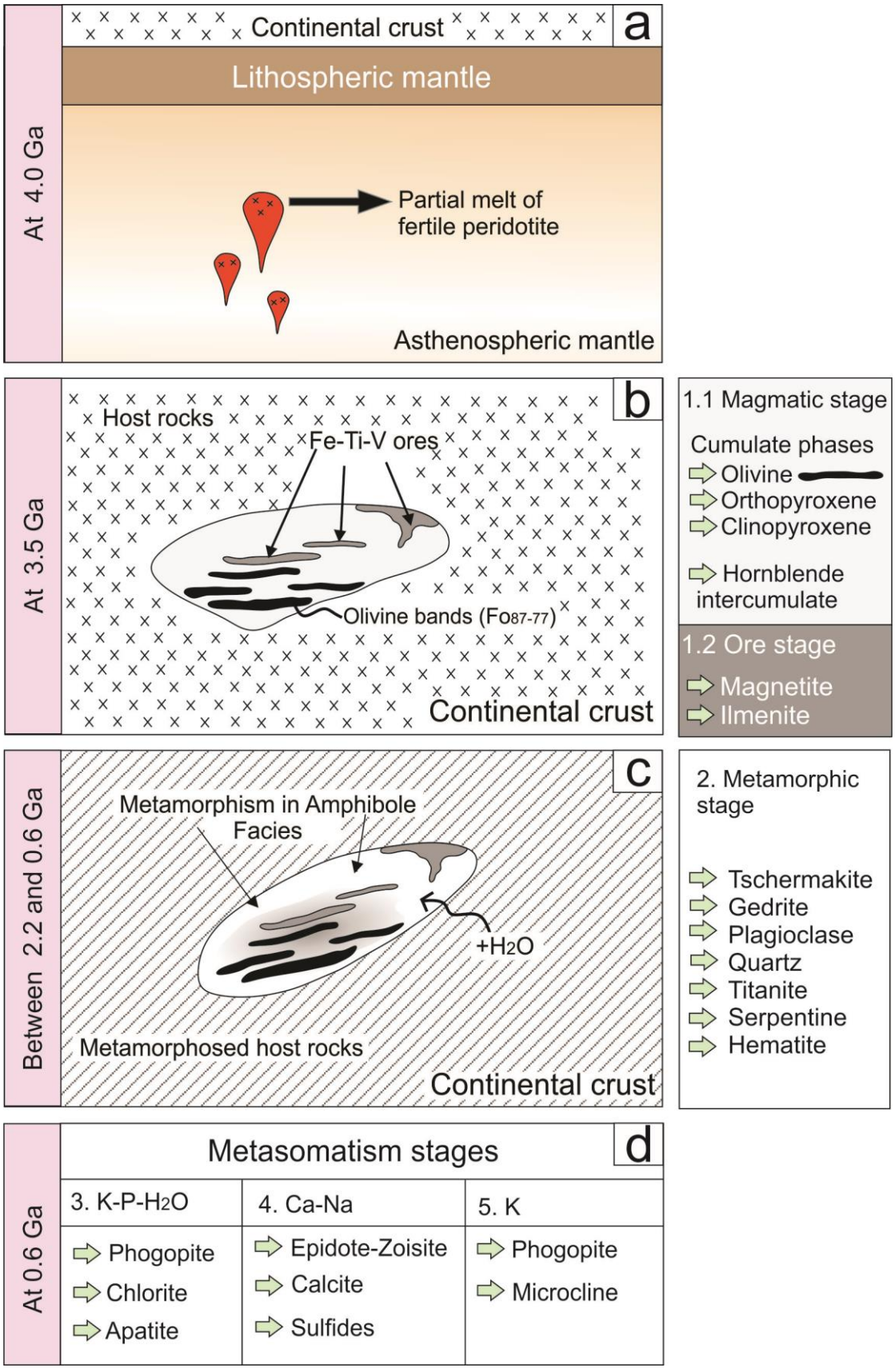

Fig. 20. Schematic model for the evolution of the layered mafic-ultramafic bodies of Sao Tomé.

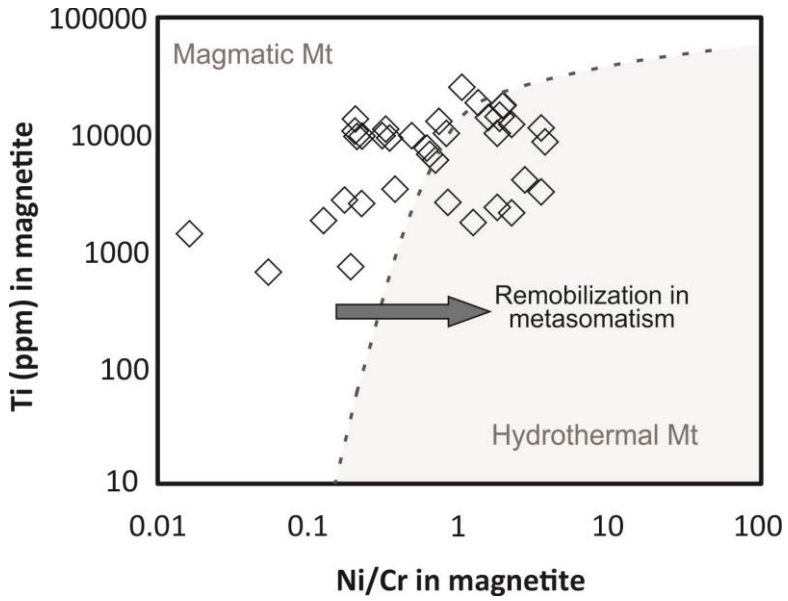

Fig. 21. Plot of Ti (ppm) versus Ni/Cr ratio (un-normalized) in magnetite (Mt) to distinguish magmatic and hydrothermal settings in the layered mafic-ultramafic bodies of São Tomé. Modifier after (Dare et al. 2014).

Table 7. Comparative list between the layered mafic-ultramafic bodies of São Tome and some layered mafic intrusions in the world.

Layered mafic intrusion	Location	Age	Rock type	Ore minerals	References
Layered mafic-ultramafic bodies of São Tomé	Rio Grande Do Norte (Brazil)	3.5 Ga (U/Pb)	Ol-Websterite and clinopyroxenite to hornblendite	Magnetite and ilmenite	
Sill of The Jacaré River	Bahia, Brazil	2,8 Ga (Sm/Nd)	Peridotite to gabbro and anorthosite	Magnetite, ilmenite, PGE, sulphides and arsenides.	(Brito, 2000)
Stillwater Complex	Montana, (USA)	2.7 Ga (Sm/Nd)	Peridotite and bronzitite to anorthosite and norite	Chromite, Platinum-group elements (PGE), sulphides, tellurides and arsenides.	(McCallum, 1996; Charlier, Namur, Latypov, et al. 2015)
Bushveld Complex	South Africa	2.06 Ga (U/Pb)	Dunite and pyroxenite to anorthosite and pure oxide layers	PGE, chromite, base metal sulphides, magnetite and ilmenite.	(Cawthorn and Walraven, 1998; Eales and Cawthorn, 1996; Hatton, 1995)
Emeishan Large Igneous Province	SW China	260 Ma (U-Pb)	Clinopyroxenite and troctolite to leucogabbro and flood basalt	Cu–Ni–(PGE) sulfide, magnetite and ilmenite	(Liu et al., 2015; Pang et al., 2008; Zhou et al., 2005)
Skaergaard intrusion	East Greenland	55 Ma (Rb/Sr)	Wehrlite and Ol-gabbro to ferrodiorites and felsic pegmatites	Cu-Fe sulphides and Gold	(Charlier et al., 2015; McBirney, 1996)

7.5. Layered bodies of São Tomé as part of São José do Campestre Massif?

The layered bodies of São Tomé report an age of crystallization U-Pb in zircon of 3.5 Ga (Fig. 18), age that corresponds to the first record of Paleoarquean rocks in the Seridó Belt. This age is closed to the 3.4 Ga, reported for the Gneiss Bom Jesus located ~50 km to the east in the São José do Campestre Massif by Dantas et al., (2004), The difference with this unit consist that this gneiss was intense contaminated with older continental crust (Dantas et al., 2014) reaching an ξNd(0) of -38.7 (table 6). Thus, these paleoarchean units had different magmatic processes and therefore different origins, which is recommended to conclude with next work focused on geochemistry. After these successive periods of Archean magmatism with different signatures of contaminations, the units were amalgamated to the supercontinent Atlántica in the paleoproterozoic, (Neves, 2003; Neves, 2011), and finally, were divided by the Picuí-João Câmara fault in the formation of the Rio Grande do Norte Domain at 600 Ma (de Sa et al., 1995; Delgado, 2000), placing in the Seridó Belt the oldest record of rocks of the Borborema Province.

In the Lajes sheet (Costa and Dantas, 2014), the Brazilian Geological Survey reports that the basement of the layered bodies of São Tomé corresponds to the Caicó Complex, emplaced at 2.2 Ga (De Souza et al., 2007), but as we have shown this paper, the ages obtained display Paleoarquean ages. Isotopic and petrographic results may correlated the basement with the Sao José do Campestre Massif, however, is recommended to carry out future works focused in geochemistry to clarify the Paleoarquean history and its relationship with the São José do Campestre Massif. Even though, the layered mafic-ultramafic bodies of São Tomé and its basement display the same age of crystallization, mineral chemistry and Sm-Nd isotopic results showed that had a different genesis, which means that both lithology's are coeval and the layered bodies are allochthonous, fact that can be explain by its immersion in the Santa Mónica shear zone.

It is important to bear in mind that during the conformation of the Borborema Province, different Fe-Ti deposits were formed throughout the time, which includes: (1) the Floresta and Bodocó deposit (Fe- Ti-V ± Cu ± Cr) in the transverse zone (Lages and Dantas, 2016), (2) the Jurema mafic-ultramafic complex (Fe-Ti-V ± Co) in the Transversal Zone (Lima et al., 2016), and also is important to include the Fe-Ti-V deposit of the Rio Jacaré Sill in the São Francisco Craton (Brito, 2000) due to the relationship with the Borborema Province.

8. Conclusions

The main results of this paper can be summarized as follows.

- Major and trace elements present in mafic minerals as olivine, pyroxene and amphibole, as well as U-Pb and Sm-Nd isotopic analyses suggests that the layered mafic-ultramafic bodies of São Tomé were generated from a partial melt of a fertile peridotite source at 4.0 Ga, which generate a ferropicritic or ferrobasaltic magma that crystalized at 3.5 Ga, been the first record of a Paleoarchean unit in the Seridó Belt and at the same time the oldest record of continental growth in the South American platform.
- An intense fractional crystallization that triggered an immiscibility process was the responsible mechanism to form Fe-Ti-V oxides ores, this occurred under a very low oxygen fugacity. The metallogenesis not involved the formation of aluminum-silicate rocks as anortosite due to the high content of volatiles in the magmatic chamber, reaching its immiscibility in an early stage of differentiation, which is a singular feature that added to its old age, differentiate the occurrence with other deposits around the world.
- After the magmatic-ore stage, both the layered bodies of São Tomé as its basement undergoes an intense metamorphism in amphibole facies between 2.2 Ga to 0.6 Ga, which oxided the ore body. In this period, the layered intrusion was amalgamated with the Sao Jose do Campestre Massif but which then were divided by the Picuí-João Câmara fault at 600 Ma, fact that is recommended to carry out future works to clarify the Paleoarquean history and its relationship with the São José do Campestre Massif.
- Finally, subsequent to the igneous and metamorphic stage, began three metasomatic stages. A K-P-H_2O stage which forms phlogopite, apatite and chlorite. Then a Ca-Na stage that forms epidote group minerals and sulfides plus titanite and calcite, and a final high temperature K-rich stage, that forms phlogopite and microcline. This intense metasomatism led to remobilized Fe, Ti, Ni and Cr in the ores while vanadium remained immobile.

9. References

Albarède, F. et al., 2004. Precise and accurate isotopic measurements using multiple-collector ICPMS. *Geochimica et Cosmochimica Acta*, 68(12), pp.2725–2744.

Almeida, F.F.M. et al., 1981. Brazilian structural provinces: An introduction. *Earth-Science Reviews*, 17(1–2), pp.1–29.

Andersen, D.J. & Lindsley, D.H., 1988. Internally consistent solution models for Fe-Mg-Mn-Ti oxides: Fe-Ti oxides. *American Mineralogist*, 7, pp.714–726.

Andersen, D.J., Lindsley, D.H. & Davidson, P.M., 1993. QUILF: A pascal program to assess equilibria among Fe-Mg-Mn-Ti oxides, pyroxenes, olivine, and quartz. *Computers & Geosciences*, 19(9), pp.1333–1350.

Arthaud, M.H. et al., 2008. Geology of the northern Borborema Province, NE Brazil and its correlation with Nigeria, NW Africa. *Geological Society, London, Special Publications*, 294(1), pp.49–67. Available at: http://sp.lyellcollection.org/content/294/1/49%5Cnhttp://sp.lyellcollection.org/content/294/1/49.abstract.

Balan, E. et al., 2006. The oxidation state of vanadium in titanomagnetite from layered basic intrusions. *American Mineralogist*, 91, pp.953–956.

Best, M.G., 2003. *Igneous and Metamorphic Petrology* 2 Rev ed. J. W. and S. Ltd, ed.,

Brito, R.S.C. de, 2000. *Geologia e petrologia do sill máfico ultramáfico do Rio Jacaré-Bahia e estudo das mineralizações de Fe-Ti-V e platinoides associadas*. Universidade de Brasília.

Bühn, B. et al., 2009. High spatial resolution analysis of Pb and U isotopes for geochronology by laser ablation multi-collector inductively coupled plasma mass spectrometry. *Annals of the Brazilian Academy of Sciences*, 81, pp.99–114.

Cawthorn, R.G., 1996. *Layered intrusions*, Elsevier.

Cawthorn, R.G. & Walraven, F., 1998. Emplacement and Crystallization Time for the Bushveld Complex. *Journal of Petrology*, 39(9), pp.1669–1687.

Chambers, J.A. & Kohn, M.J., 2012. Titanium in muscovite, biotite, and hornblende: Modeling, thermometry, and rutile activities of metapelites and amphibolites. *American Mineralogist*, 97, pp.543–555.

Charlier, B., Namur, O., Bolle, O., et al., 2015. Fe – Ti – V – P ore deposits associated with Proterozoic massif-type anorthosites and related rocks. *Earth Science Reviews*, 141, pp.56–81. Available at: http://dx.doi.org/10.1016/j.earscirev.2014.11.005.

Charlier, B., Namur, O., Latypov, R., et al., 2015. *Layered Intrusions*, Springer.

Charlier, B. & Grove, T.L., 2012. Experiments on liquid immiscibility along tholeiitic liquid lines of descent. *Contributions to Mineral Petrology*, 164, pp.27–44.

Costa, A. & Dantas, A., 2014. Programa Geologia do Brasil-PGB. Lajes. Folha SB.24-X-D-VI. Estado do Rio Grande do Norte. Carta Geológica e de Recursos Minerais. 1 mapa colorido, 90,00 x 70,00cm. Escala 1:100.000. , p.1.

Costa, A.P. et al., 2014. Petrographic characterization with QEMSCAN analysis of Fe-Ti

occurrence associated with ultramafic rocks in São Tomé, Brazil. *VI Simpósio Brasileiro de Exploração Mineral*, p.4.

Dantas, E.L. et al., 2014. Crustal growth in the 3.4-2.7 Ga São José de Campestre Massif, Borborema Province, NE Brazil. *Precambrian Research*, 227, pp.120–156. Available at: http://dx.doi.org/10.1016/j.precamres.2012.08.006.

Dantas, E.L. et al., 2004. The 3.4-3.5 Ga São José do Campestre massif, NE Brazil: Remnants of the oldest crust in South America. *Precambrian Research*, 130(1–4), pp.113–137.

Dare, S.A.S. et al., 2014. Trace elements in magnetite as petrogenetic indicators. *Mineralium Deposita*, 49(7), pp.785–796.

Deer, W.A., Howie, R.A. & Zussman, J., 1986. *An introduction to the rock-forming minerals* 17th ed. Longman group, ed.,

Delgado, I.M. et al., 2003. Bacias Neoproterozóicas e Cambro-Ordovicianas. In *Geotectônica do Escudo Atlântico*. Serviço Geológico do Brasil (CPRM), p. 334.

DePaolo, D.J., 1981. Neodymium isotopes in the Colorado Front Range and implications for crust formation and mantle evolution in the Proterozoic. *Nature*, 291, pp.193–197.

Dupuis, C. & Beaudoin, G., 2011. Discriminant diagrams for iron oxide trace element fingerprinting of mineral deposit types. *Mineralium Deposita*, 46(4), pp.319–335.

Eales, H.V. & Cawthorn, R.G., 1996. The Bushveld Complex. In *Layered Intrusions*. Elsevier Science, p. 530.

Fleet, M., 1981. The structure of magnetite. In *Acta Crystallogr.* pp. 917–920.

Ghiorso, M.S. & Sack, O., 1991. Fe-Ti oxide geothermometry: thermodynamic formulation and the estimation of intensive variables in silicic magmas. *Contributions to Mineralogy and Petrology*, 108(4), pp.485–510.

Gioia, S.M.C.L. & Pimentel, M.M., 2000. The Sm-Nd isotopic method in the geochronology laboratory of University of Brasilia. *Anais da Academia Brasileira de Ciências*, 72(2), pp.219–245.

Harley, S.L., Kelly, N.M. & Möller, A., 2007. Zircon Behaviour and the Thermal Histories of Mountain Chains. *Elements*, 3, pp.25–30.

Hatton, C.J., 1995. The Bushveld Complex , a product of interaction among magmas derived from a mantle plume. *Communs geol. Surv. Namibia*, 10, pp.93–98.

Henry, D.J., Guidotti, C. V. & Thomson, J.A., 2005. The Ti-saturation surface for low-to-medium pressure metapelitic biotites: Implications for geothermometry and Ti-substitution mechanisms. *American Mineralogist*, 90, p.316—328.

Herzberg, C. et al., 2013. Nickel and helium evidence for melt above the core-mantle boundary. *Nature*, 493(7432), pp.393–397. Available at: http://dx.doi.org/10.1038/nature11771.

Herzberg, C., Vidito, C. & Starkey, N.A., 2016. Nickel – cobalt contents of olivine record origins of mantle peridotite and related rocks. *American Mineralogist*, 101, pp.1952–1966.

Hey, M.H., 1954. A new review of the chlorites. *Journal of the mineralogical society*, 30, pp.277–292.

Hollanda, M.H.B.M. et al., 2015. Detrital zircon ages and Nd isotope compositions of the Seridó

and Lavras da Mangabeira basins (Borborema Province , NE Brazil): Evidence for exhumation and recycling associated with a major shift in sedimentary provenance Brasiliano/Pan African basement . *Precambrian Research*, 258, pp.186–207. Available at: http://dx.doi.org/10.1016/j.precamres.2014.12.009.

Hollanda, M.H.B.M. et al., 2011. Long-lived Paleoproterozoic granitic magmatism in the Seridó-Jaguaribe domain, Borborema Province-NE Brazil. *Journal of South American Earth Sciences*, 32(4), pp.287–300. Available at: http://dx.doi.org/10.1016/j.jsames.2011.02.008.

Hou, T. et al., 2017. ScienceDirect Experimental study of liquid immiscibility in the Kiruna-type Vergenoeg iron – fluorine deposit, South Africa. *Geochimica et Cosmochimica Acta*, 203, pp.303–322.

Jackson, S.E. et al., 2004. The application of laser ablation-inductively coupled plasma-mass spectrometry to in situ U–Pb zircon geochronology. *Chemical Geology*, 211(1–2), pp.47–69.

Lages, G. de A., 2014. *Os complexos máfico-ultrameaficos mineralizados (Fe-Ti±V±Cu±Cr) de Floresta e Bodocó na porção ocidental da Província Borborema e suas implicações geodinâmicas para a evolução da parte oeste da Zona Transversal*. Universidade de Brasilia.

Lages, G.D.A. & Dantas, E.L., 2016. Floresta and Bodocó Mafic – Ultramafic Complexes, western Borborema Province, Brazil: Geochemical and isotope constraints for evolution of a Neoproterozoic arc environment and retro-eclogitic hosted. *Precambrian Research*, 280, pp.95–119. Available at: http://dx.doi.org/10.1016/j.precamres.2016.04.017.

Leake, B.E. et al., 1997. Nomenclature of Amphiboles: Report of the Subcommittee on Amphiboles of the International Mineralogical Association Commission on New Minerals and Mineral Names. *Mineralogical magazine*, 61, pp.295–321.

Lester, G.W. et al., 2013. Experiments on liquid immiscibility in silicate melts with H2O, P, S, F and Cl: implications for natural magmas. *Contributions to Mineral Petrology*, 166, pp.329–349.

Lima, F.J. da C. et al., 2016. O Complexo Máfico-Ultramáfico Jurema: descoberta de corpo mineralizado em Fe-Ti ± V ± Co em Betânia, Pernambuco, Zona Transversal, Província Borborema. *Serviço Geológico do Brasil (CPRM)*, 6, p.8.

Liu, P. et al., 2015. In-situ LA-ICP-MS trace elemental analyses of magnetite: Fe – Ti – (V) oxide-bearing mafic – ultramafic layered intrusions of the Emeishan Large Igneous Province , SW China. *Ore Geology Reviews*, 65, pp.853–871. Available at: http://dx.doi.org/10.1016/j.oregeorev.2014.09.002.

Ludwig, K.R., 2008. User â€™s Manual for Isoplot 3.70. A geochronological Toolkit for Microsoft Excel. *Berkeley Geochronology Center*, 4(4), p.76.

Martin, H., 1986. Effect of steeper Archean geothermal gradient on geochemistry of subduction-zone magmas. *Geology*, 14, pp.753–756.

McBirney, A.R., 1996. The Skaergaard Intrusion. In *Layered Intrusions*. Elsevier Science, p. 530.

McCallum, I.S., 1996. The Stillwater Complex. In *Layered Intrusions*. Elsevier Science, p. 530.

McDougall, I. & Harrison, T., 1999. *Geochronology and thermochronology by the 40Ar/39Ar method* 2nd ed., Oxford: Oxford University Press.

Nadoll, P. et al., 2014. The chemistry of hydrothermal magnetite: A review. *Ore Geology Reviews*, 61, pp.1–32. Available at: http://dx.doi.org/10.1016/j.oregeorev.2013.12.013.

Do Nascimento, M.A.L., Galindo, A.C. & de Medeiros, V.C., 2015. Ediacaran to Cambrian magmatic suites in the Rio Grande do Norte domain, extreme Northeastern Borborema Province (NE of Brazil): Current knowledge. *Journal of South American Earth Sciences*, 58, pp.281–299. Available at: http://dx.doi.org/10.1016/j.jsames.2014.09.008.

Neves, S.P., 2011. Atlantica revisited: new data and thoughts on the formation and evolution of a long-lived continent. *International Geology Review*, 53(11–12), pp.1377–1391.

Neves, S.P., 2003. Proterozoic history of the Borborema province (NE Brazil): Correlations with neighboring cratons and Pan-African belts and implications for the evolution of western Gondwana. *Tectonics*, 22(4).

Pang, K. et al., 2008. Origin of Fe-Ti Oxide Ores in Mafic Intrusions: Evidence from the Panzhihua Intrusion , SW China. *Journal of Petrology*, 49(2), pp.295–313.

Pearson, D.G. et al., 1995. Stabilisation of Archaean lithospheric mantle: A Re-0s isotope study of peridotite xenoliths from the Kaapvaal craton. *Earth and Planetary Science Letters*, 134, pp.341–357.

Peltonen, P. et al., 2006. Multi-stage origin of the lower crust of the Karelian craton from 3.5 to 1.7 Ga based on isotopic ages of kimberlite-derived mafic granulite xenoliths. *Precambrian Research*, 147, pp.107–123.

Rollinson, H., 2010. Coupled evolution of Archean continental crust and subcontinental lithospheric mantle. *Geology*, (12), pp.1083–1086.

Rollinson, H., 1993. *Using Geochemical Data: Evaluation, Presentation, Interpretation* Routledge, ed., New York: Longman Geochemistry Series.

Rubatto, D., 2002. Zircon trace element geochemistry: partitioning with garnet and the link between U – Pb ages and metamorphism. *Chemical geology*, 184, pp.123–138.

de Sa, E.F.J. et al., 1995. Pre-Brasiliano orogenic evolution in the Serido Belt, NE Brazil; conflicting geochronological and structural data. *Revista Brasileira de Geociencias*, 25(4), pp.307–314.

Van Schmus, W.R. et al., 2003. The Seridó Group of NE Brazil, a late Neoproterozoic pre- to syn-collisional basin in West Gondwana: Insights from SHRIMP U-Pb detrital zircon ages and Sm-Nd crustal residence (TDM) ages. *Precambrian Research*, 127(4), pp.287–327.

De Souza, Z.S. et al., 2007. Calc-alkaline magmatism at the Archean-Proterozoic transition: The Caicó Complex Basement (NE Brazil). *Journal of Petrology*, 48(11), pp.2149–2185.

Souza Neto, J.A. et al., 2008. W-Au skarns in the Neo-Proterozoic Seridó Mobile Belt, Borborema Province in northeastern Brazil: An overview with emphasis on the Bonfim deposit. *Mineralium Deposita*, 43(2), pp.185–205.

Toplis, M.J. & Corgne, A., 2002. An experimental study of element partitioning between

magnetite , clinopyroxene and iron-bearing silicate liquids with particular emphasis on vanadium. *Contributions to Mineralogy and Petrology*, 144, pp.22–37.

Vantongeren, J.A. & Mathez, E.A., 2012. Large-scale liquid immiscibility at the top of the Bushveld Complex , South Africa. *Geology*, 40(6), pp.491–494.

Vasconcelos, P.M. et al., 2002. 40Ar/39Ar geochronology at the Instituto de Geociências , USP: instrumentation , analytical procedures , and calibration. *Annals of the Brazilian Academy of Sciences*, 74, pp.297–342.

Vauchez, A. et al., 1995. The Borborema shear zone system, NE Brazil. *Journal of South American Earth Sciences*, 8(3–4), pp.247–266.

Winter, J.D., 2001. *An introduction to igneous and metamorphic petrology*, Prentice-Hall.

Wones, D.R. & Eugster, H.P., 1965. Stability of biotite: Experiment, theory, and application. *American Mineralogist*, 50, pp.1228–1272.

Wyllie, P.J., 1992. Experimental Petrology: Earth Materials Science. In *Understanding the Earth*. pp. 67–87.

Zhou, M. et al., 2005. Geochemistry, Petrogenesis and Metallogenesis of the Panzhihua Gabbroic Layered Intrusion and Associated Fe – Ti – V Oxide Deposits , Sichuan Province, SW China. *Journal of Petrology*, 46(11), pp.2253–2280.

ANEXOS

Tabela A8. Química mineral das olivinas estudadas.

Sample	Vela-008				Vela-021				VELA-029															
SiO_2	39.15	38.71	39.23	38.66	39.02	38.79	38.92	38.37	39.62	39.00	39.46	39.28	39.80	38.85	39.66	40.18	40.20	40.23	39.70	40.23	40.68	40.55	40.34	40.08
TiO_2	0.00	0.00	0.00	0.11	0.00	0.00	0.00	0.00	0.00	0.05	0.09	0.12	0.19	0.00	0.03	0.05	0.00	0.08	0.04	0.00	0.00	0.00	0.00	0.00
Al_2O_3	0.00	0.02	0.01	0.02	0.01	0.00	0.00	0.00	0.05	0.00	0.00	0.03	0.01	0.03	0.00	0.03	0.01	0.01	0.01	0.01	0.03	0.00	0.00	0.00
Cr_2O_3	0.00	0.01	0.00	0.00	0.04	0.00	0.07	0.01	0.07	0.04	0.02	0.00	0.06	0.00	0.00	0.06	0.01	0.01	0.00	0.00	0.04	0.01	0.01	0.00
FeO	19.32	19.34	19.47	19.51	20.59	20.27	19.19	19.20	11.97	12.77	12.30	12.45	12.43	12.23	11.87	12.04	12.25	12.68	12.92	12.21	12.74	12.71	13.07	13.08
MnO	0.39	0.16	0.24	0.24	0.16	0.27	0.45	0.42	0.22	0.26	0.13	0.15	0.33	0.23	0.23	0.23	0.17	0.30	0.29	0.12	0.17	0.12	0.24	0.31
MgO	40.80	40.73	40.91	40.88	40.03	40.44	40.78	40.66	46.09	45.93	45.91	45.74	46.45	46.45	46.56	46.33	45.82	45.66	46.11	46.60	46.65	46.09	46.36	45.92
NiO	0.39	0.32	0.39	0.40	0.33	0.26	0.36	0.46	0.44	0.48	0.52	0.47	0.39	0.56	0.48	0.37	0.47	0.59	0.48	0.48	0.48	0.56	0.55	0.48
CaO	0.01	0.02	0.04	0.02	0.02	0.00	0.00	0.01	0.03	0.02	0.00	0.00	0.00	0.02	0.02	0.00	0.02	0.00	0.00	0.03	0.03	0.01	0.02	0.02
Total	100.06	99.31	100.28	99.85	100.20	100.03	99.76	99.14	98.48	98.54	98.43	98.25	99.64	98.38	98.86	99.29	98.94	99.56	99.54	99.67	100.81	100.05	100.61	99.88
Number of cations on the basis of 4 oxygen																								
Si	1.00	1.00	1.00	1.00	1.00	1.00	1.00	1.00	1.00	0.99	1.00	1.00	0.99	0.98	1.00	1.00	1.01	1.01	0.99	1.00	1.00	1.01	1.00	1.00
$Fe_{(ii)}$	0.41	0.42	0.42	0.42	0.44	0.44	0.41	0.42	0.25	0.27	0.26	0.26	0.26	0.26	0.25	0.25	0.26	0.26	0.27	0.25	0.26	0.26	0.27	0.27
Mn	0.01	0.00	0.01	0.01	0.00	0.01	0.01	0.01	0.00	0.01	0.00	0.00	0.01	0.00	0.00	0.00	0.00	0.01	0.01	0.00	0.00	0.00	0.01	0.01
Mg	1.56	1.57	1.56	1.57	1.54	1.55	1.56	1.57	1.73	1.73	1.73	1.73	1.73	1.75	1.74	1.72	1.71	1.70	1.72	1.73	1.72	1.71	1.71	1.71
Ni	0.01	0.01	0.01	0.01	0.01	0.01	0.01	0.01	0.01	0.01	0.01	0.01	0.01	0.01	0.01	0.01	0.01	0.01	0.01	0.01	0.01	0.01	0.01	0.01
Sum	3.00	3.00	3.00	3.00	3.00	3.00	3.00	3.00	3.00	3.01	3.00	3.00	3.00	3.02	3.00	2.99	2.99	2.99	3.00	3.00	3.00	2.99	3.00	3.00
Fo	78.68	78.83	78.72	78.67	77.48	77.83	78.73	78.69	87.08	86.27	86.82	86.61	86.65	86.92	87.28	87.06	86.80	86.24	86.15	87.08	86.57	86.49	86.13	85.95
Fa	20.89	21.00	21.01	21.06	22.35	21.88	20.78	20.84	12.69	13.45	13.05	13.23	13.01	12.84	12.48	12.69	13.02	13.43	13.54	12.80	13.26	13.38	13.62	13.73
Ni ppm	3065	2538	3033	3104	2570	2020	2813	3591	3473	3733	4086	3709	3025	4424	3748	2931	3685	4605	3764	3764	3803	4393	4330	3733

Tabela A9. Química mineral dos piroxenos estudados.

Mineral/Rock type	Augita																		Enstatita			
	Clinopiroxenito						Ol-Websterito						Ol-Websterito						Clinopiroxenito		Hbl-piroxenito		Ol-Websterito	
Sample	Vela-007						Vela-008						Vela-021						Vela-025		Vela-030B		Vela-008	
SiO2	55.26	54.27	53.35	53.94	54.57	53.96	56.99	55.07	52.24	56.94	56.73	54.40	57.06	56.83	57.55	57.57	58.39	56.65	54.87	54.35	54.68	54.05	49.39	48.05
TiO2	0.17	0.13	0.12	0.20	0.00	0.25	0.46	0.34	0.16	0.02	0.04	0.22	0.22	0.18	0.23	0.13	0.12	0.19	0.13	0.20	0.00	0.19	0.00	0.19
Al2O3	2.82	4.42	5.30	4.71	4.03	3.66	1.52	3.10	2.82	0.67	1.88	3.67	1.51	1.74	1.37	1.63	0.85	2.06	1.57	2.08	1.28	0.02	0.02	0.02
Cr2O3	0.09	0.01	0.04	0.00	0.07	0.09	0.00	0.36	0.64	0.03	0.00	0.20	0.00	0.00	0.00	0.00	0.08	0.05	0.14	0.04	0.00	0.00	0.03	0.00
Fe2O3	0.00	0.00	0.00	0.00	0.00	0.00	0.00	0.00	0.00	0.00	0.00	0.00	0.00	0.00	0.00	0.00	0.00	0.00	0.00	0.00	0.00	3.82	6.03	14.01
FeO	10.11	6.65	7.09	6.54	7.76	6.54	3.70	4.35	4.33	4.99	4.00	4.73	3.94	3.89	3.71	3.90	3.53	4.10	4.99	5.65	21.56	12.33	18.84	5.15
MnO	0.48	0.30	0.32	0.25	0.52	0.28	0.22	0.12	0.13	0.12	0.10	0.09	0.09	0.19	0.01	0.03	0.09	0.03	0.14	0.06	0.57	0.35	0.53	0.35
MgO	20.90	19.88	19.18	19.17	19.79	19.61	22.59	21.43	19.88	23.44	22.08	21.43	22.44	21.66	22.54	22.09	22.52	21.99	21.44	21.69	19.10	29.03	22.12	29.03
CaO	7.87	12.24	12.25	12.47	10.77	11.84	12.64	12.56	12.61	11.39	12.32	12.10	12.88	12.60	12.80	12.76	12.81	12.72	11.62	11.41	0.91	0.27	0.06	0.27
Na2O	0.52	0.66	0.88	0.77	0.71	0.50	0.30	0.51	0.66	0.14	0.33	0.80	0.19	0.25	0.30	0.24	0.06	0.27	0.21	0.33	0.48	0.00	0.04	0.00
K2O	0.02	0.09	0.07	0.08	0.07	0.07	0.05	0.05	0.22	0.02	0.05	0.03	0.02	0.04	0.02	0.03	0.01	0.09	0.04	0.04	0.11	0.00	0.00	0.00
Total	98.23	98.66	98.59	98.11	98.27	96.81	98.47	97.89	93.70	97.76	97.52	97.67	98.35	97.38	98.52	98.38	98.46	98.14	95.15	95.85	98.70	100.05	97.05	97.07
Number of cations on the basis of 6 oxygen																								
Si	2.01	1.96	1.94	1.96	1.98	1.99	2.03	1.99	1.98	2.05	2.04	1.97	2.04	2.05	2.05	2.05	2.07	2.03	2.03	2.01	2.05	1.96	1.94	1.86
Al (iv)	-0.01	0.04	0.06	0.04	0.02	0.01	-0.03	0.01	0.02	-0.05	-0.04	0.03	-0.04	-0.05	-0.05	-0.05	-0.07	-0.03	-0.03	-0.01	-0.05	0.00	0.00	0.00
Al	0.13	0.15	0.17	0.16	0.16	0.14	0.10	0.12	0.11	0.08	0.12	0.13	0.10	0.12	0.11	0.12	0.11	0.12	0.10	0.10	0.11	0.00	0.00	0.00
Fe(iii)	0.00	0.00	0.00	0.00	0.00	0.00	0.00	0.00	0.00	0.00	0.00	0.00	0.00	0.00	0.00	0.00	0.00	0.00	0.00	0.00	0.00	0.10	0.18	0.39
Cr	0.00	0.00	0.00	0.00	0.00	0.00	0.00	0.01	0.02	0.00	0.00	0.01	0.00	0.00	0.00	0.00	0.00	0.00	0.00	0.00	0.00	0.00	0.00	0.00
Ti	0.00	0.00	0.00	0.01	0.00	0.01	0.01	0.01	0.00	0.00	0.00	0.01	0.01	0.00	0.01	0.00	0.00	0.00	0.00	0.01	0.00	0.01	0.00	0.01
Fe(ii)	0.31	0.20	0.22	0.20	0.24	0.20	0.11	0.13	0.14	0.15	0.12	0.14	0.12	0.12	0.11	0.12	0.11	0.12	0.16	0.18	0.69	0.37	0.61	0.16
Mn	0.01	0.01	0.01	0.01	0.02	0.01	0.01	0.00	0.00	0.00	0.00	0.00	0.00	0.01	0.00	0.00	0.00	0.00	0.00	0.00	0.02	0.01	0.02	0.01
Mg	1.13	1.07	1.04	1.04	1.07	1.08	1.20	1.15	1.12	1.26	1.18	1.16	1.20	1.16	1.20	1.17	1.19	1.17	1.19	1.19	1.07	1.57	1.30	1.67

Mineral/Rock type	Augita																				Enstatita			
	Clinopiroxenito						Ol-Websterito						Ol-Websterito						Clinopiroxenito		Hbl-piroxenito		Ol-Websterito	
Sample	Vela-007						Vela-008						Vela-021						Vela-025		Vela-030B		Vela-008	
Ca	0.31	0.47	0.48	0.49	0.42	0.47	0.48	0.49	0.51	0.44	0.48	0.47	0.49	0.49	0.49	0.49	0.49	0.49	0.46	0.45	0.04	0.01	0.00	0.01
Na	0.04	0.05	0.06	0.05	0.05	0.04	0.02	0.04	0.05	0.01	0.02	0.06	0.01	0.02	0.02	0.02	0.00	0.02	0.02	0.02	0.04	0.00	0.00	0.00
Sum	3.95	3.97	3.98	3.96	3.96	3.95	3.94	3.95	3.97	3.94	3.93	3.97	3.93	3.92	3.93	3.92	3.91	3.93	3.94	3.96	3.95	4.03	4.05	4.12
Wo	17.36	26.97	27.37	28.03	24.02	26.60	26.79	27.35	28.80	23.71	26.61	26.47	27.21	27.40	27.17	27.37	27.23	27.29	25.52	24.74	2.02	0.52	0.12	0.50
En	64.14	60.96	59.62	59.95	61.42	61.28	66.61	64.95	63.18	67.87	66.35	65.24	66.01	65.54	66.56	65.93	66.62	65.67	65.55	65.48	59.05	76.02	61.66	74.32
Fs	18.50	12.07	13.00	12.02	14.56	12.12	6.59	7.69	8.02	8.42	7.03	8.29	6.77	7.06	6.27	6.70	6.15	7.04	8.93	9.78	38.93	23.47	38.22	25.17
WEF	100	100	100	100	100	100	100	1000	100	100	100	100	100	100	100	100	100	100	100	100	100	100	100	100

Tabela A10. Química mineral dos anfibólios estudados.

Rock type	Gbro	Gbro	Gbro	Gbro	Gbro	Hpxt	Hpxt	Clfe	Clfe	Clfe	Clfe	Hblt	Gbro	Owb	Owb	Owb	Owb	Owb	Owb
Sample	Vela-006-1	Vela-006-3	Vela-006-3	Vela-012-1	Vela-012-2	Vela-030B-1	Vela-030B-2	Vela-002-1	Vela-002-2	Vela-002-3	Vela-002-4	Vela-017B-1	Vela-006-3	Vela-021-1	Vela-021-2	Vela-021-3	Vela-021-4	Vela-021-5	Vela-021-6
	Tschermakite							Mg-Hornblende						Magnesio-gedrite					
SiO2	42.62	43.84	44.27	42.97	42.97	43.69	44.29	52.47	51.35	48.79	47.66	44.43	45.11	40.77	41.41	42.37	42.00	41.37	41.61
TiO2	0.87	0.80	0.61	0.73	0.78	0.42	0.56	0.29	0.47	0.41	0.58	0.63	0.49	0.11	0.00	0.09	0.09	0.04	0.01
Al2O3	13.08	11.76	11.53	12.52	12.84	12.86	12.24	6.81	7.11	9.20	9.69	11.35	14.68	18.61	18.23	16.63	17.67	18.90	18.74
Cr2O3	0.02	0.10	0.03	0.00	0.04	0.24	0.07	0.08	0.00	0.00	0.09	0.00	0.00	0.21	0.21	0.16	0.13	0.26	0.15
Fe2O3	9.46	10.11	9.72	6.92	7.30	8.53	9.95	2.85	4.13	3.20	1.68	4.69	3.49	6.90	6.75	6.46	6.80	6.94	7.17
FeO	8.38	7.18	7.48	11.14	10.77	7.22	6.30	4.72	3.76	5.76	7.14	11.70	12.51	0.00	0.00	0.00	0.00	0.00	0.00
MnO	0.19	0.20	0.17	0.21	0.27	0.22	0.22	0.11	0.08	0.09	0.05	0.21	0.24	0.02	0.00	0.00	0.13	0.00	0.00
MgO	10.41	11.32	11.34	9.95	9.82	11.57	11.69	18.17	17.88	16.37	16.18	11.35	8.86	31.72	32.34	32.86	32.87	31.81	32.15
NiO	0.06	0.02	0.01	0.00	0.00	0.00	0.09	0.00	0.08	0.01	0.00	0.00	0.05	0.11	0.11	0.28	0.16	0.12	0.22
CaO	10.94	10.91	10.91	11.31	11.23	11.10	10.72	13.02	12.77	12.98	12.89	12.18	9.51	0.05	0.01	0.07	0.04	0.07	0.00

Rock type	Gbro	Gbro	Gbro	Gbro	Gbro	Hpxt	Hpxt	Clfe	Clfe	Clfe	Clfe	Hblt	Gbro	Owb	Owb	Owb	Owb	Owb	Owb
Sample	Vela-006-1	Vela-006-3	Vela-006-3	Vela-012-1	Vela-012-2	Vela-030B-1	Vela-030B-2	Vela-002-1	Vela-002-2	Vela-002-3	Vela-002-4	Vela-017B-1	Vela-006-3	Vela-021-1	Vela-021-2	Vela-021-3	Vela-021-4	Vela-021-5	Vela-021-6
	Tschermakite							Mg-Hornblende						Magnesio-gedrite					
Na2O	1.64	1.47	1.44	1.68	1.63	1.73	1.56	0.54	0.49	0.73	1.29	1.64	1.54	0.00	0.00	0.00	0.00	0.00	0.00
K2O	0.41	0.27	0.26	0.41	0.41	0.29	0.24	0.08	0.06	0.25	0.59	0.36	2.48	0.03	0.05	0.01	0.02	0.02	0.00
BaO	0.00	0.00	0.00	0.00	0.00	0.00	0.07	0.00	0.00	0.00	0.07	0.00	0.00	0.00	0.00	0.05	0.00	0.00	0.00
SrO	0.00	0.00	0.00	0.06	0.00	0.00	0.11	0.03	0.00	0.00	0.06	0.00	0.00	0.01	0.10	0.06	0.04	0.01	0.00
PbO	0.00	0.00	0.00	0.00	0.00	0.00	0.00	0.00	0.00	0.00	0.00	0.00	0.00	0.00	0.00	0.00	0.00	0.00	0.00
F	0.01	0.00	0.00	0.00	0.00	0.00	0.00	0.00	0.06	0.05	0.00	0.00	0.00	0.00	0.00	0.00	0.00	0.00	0.00
Cl	0.07	0.04	0.02	0.04	0.04	0.03	0.03	0.03	0.03	0.05	0.05	0.03	0.03	0.02	0.01	0.02	0.00	0.01	0.02
H2O*	2.02	2.04	2.05	2.01	2.02	2.05	2.06	2.16	2.11	2.08	2.08	2.04	2.05	2.21	2.23	2.23	2.25	2.24	2.25
O=F,Cl	0.02	0.01	0.00	0.01	0.01	0.01	0.01	0.01	0.03	0.03	0.01	0.01	0.01	0.00	0.00	0.00	0.00	0.00	0.00
Total	100.2	100.1	99.8	100.0	100.1	99.9	100.2	101.4	100.4	100.0	100.1	100.6	101.0	100.8	101.4	101.3	102.2	101.8	102.3
Number of cations on the basis of 23 oxygen																			
Si	6.26	6.40	6.47	6.36	6.34	6.37	6.42	7.25	7.17	6.92	6.81	6.51	6.57	5.51	5.56	5.70	5.60	5.53	5.54
Al iv	1.74	1.60	1.53	1.64	1.66	1.63	1.58	0.75	0.83	1.08	1.19	1.49	1.43	2.49	2.44	2.30	2.40	2.47	2.46
Al vi	0.52	0.42	0.45	0.55	0.58	0.57	0.52	0.36	0.34	0.46	0.44	0.47	1.08	0.48	0.44	0.33	0.38	0.51	0.48
Ti	0.10	0.09	0.07	0.08	0.09	0.05	0.06	0.03	0.05	0.04	0.06	0.07	0.05	0.01	0.00	0.01	0.01	0.00	0.00
Fe3+	1.05	1.11	1.07	0.77	0.81	0.94	1.09	0.30	0.43	0.34	0.18	0.52	0.38	0.70	0.68	0.65	0.68	0.70	0.72
Fe2+	1.03	0.88	0.91	1.38	1.33	0.88	0.76	0.55	0.44	0.68	0.85	1.43	1.52	0.00	0.00	0.00	0.00	0.00	0.00
Mg	2.28	2.46	2.47	2.20	2.16	2.51	2.53	3.74	3.72	3.46	3.45	2.48	1.92	6.39	6.47	6.58	6.53	6.34	6.38
Ca	1.72	1.71	1.71	1.79	1.78	1.73	1.67	1.93	1.91	1.97	1.97	1.91	1.48	0.01	0.00	0.01	0.01	0.01	0.00
Na	0.47	0.42	0.41	0.48	0.47	0.49	0.44	0.15	0.13	0.20	0.36	0.46	0.44	0.00	0.00	0.00	0.00	0.00	0.00
K	0.08	0.05	0.05	0.08	0.08	0.05	0.04	0.01	0.01	0.05	0.11	0.07	0.46	0.00	0.01	0.00	0.00	0.00	0.00
OH	1.98	1.99	1.99	1.99	1.99	1.99	1.99	1.99	1.97	1.97	1.99	1.99	1.99	2.00	2.00	2.00	2.00	2.00	2.00
Sum	17.3	17.2	17.2	17.4	17.3	17.3	17.2	17.1	17.1	17.2	17.4	17.4	17.4	17.6	17.6	17.6	17.7	17.6	17.6

Rock code: Clfe-comformable layers of Fe-Ti-V; Gbro-Gabbro; Hblt-Hornblendite; Hpxt-Hbl-piroxenite; Owb-Ol-Websterite.